AD-A067 918 RADIATION RESEARCH ASSOCIATES INC FORT WORTH TEX F/G 18/8
CALCULATIONAL PROCEDURE FOR EVALUATING TIME- AND SPATIAL-DEPEND--ETC(U)
APR 79 M B WELLS, R B LIVESAY F08606-77-C-0008
UNCLASSIFIED RRA-T7814-I AFTAC-TR-79-22 NL

1 OF 1
ADA
067918

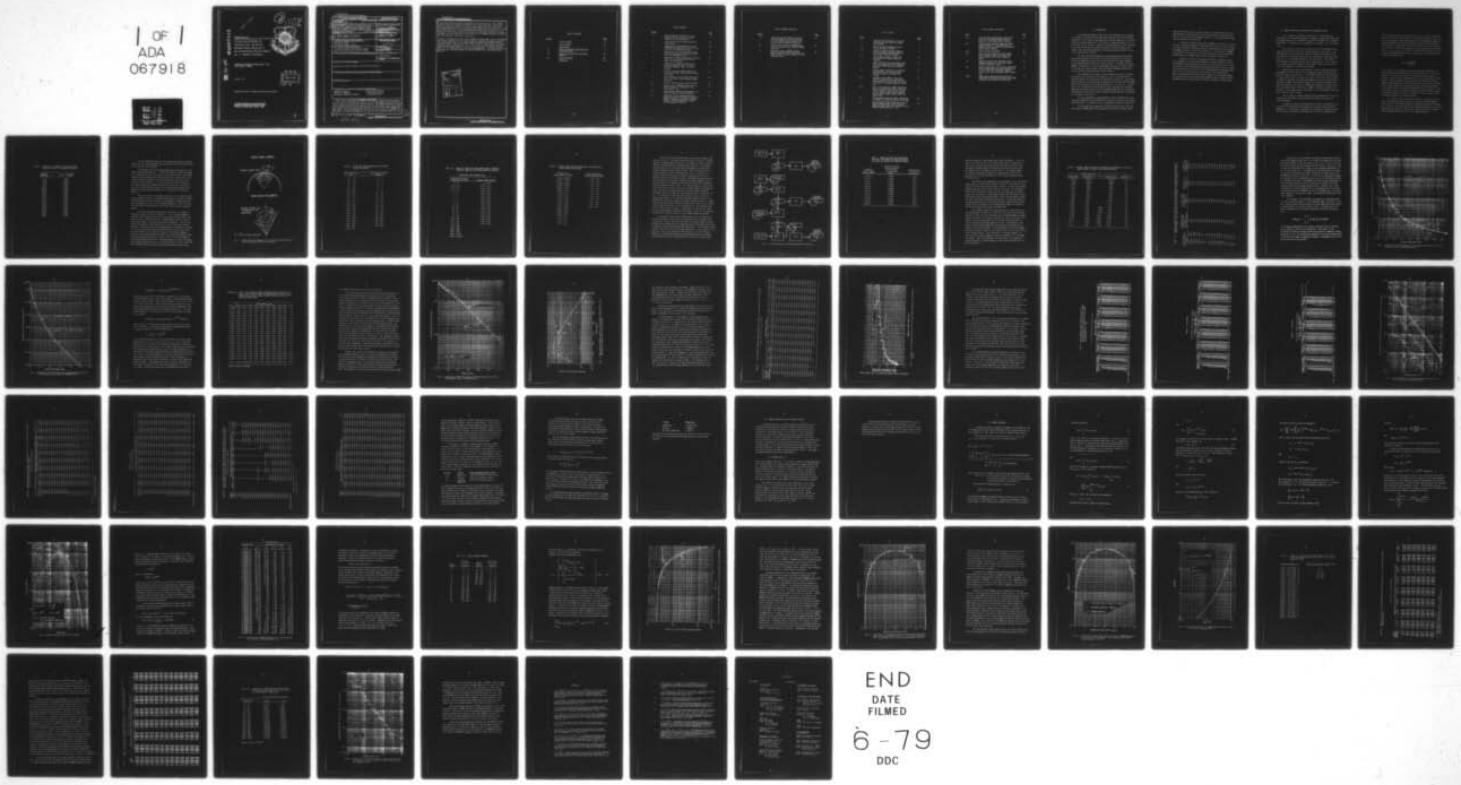

END
DATE
FILMED
6-79
DDC

AFTAC-TR-79-22

CALCULATIONAL PROCEDURE FOR EVALUATING TIME- AND SPATIAL-DEPENDENT ENERGY DEPOSITION IN AIR FOR ANISOTROPIC NUCLEAR SOURCES: VOL. I, TECHNICAL DISCUSSION

Radiation Research Associates, Inc.
Fort Worth, Texas

2 April 1979

Approved for public release, distribution unlimited

AIR FORCE TECHNICAL APPLICATIONS CENTER
HEADQUARTERS UNITED STATES AIR FORCE
PATRICK AIR FORCE BASE, FLORIDA 32925

UNCLASSIFIED

SECURITY CLASSIFICATION OF THIS PAGE (When Data Entered)

(19) **REPORT DOCUMENTATION PAGE**

READ INSTRUCTIONS BEFORE COMPLETING FORM

(18) 1. REPORT NUMBER: AFTAC-TR-79-22	2. GOVT ACCESSION NO.
3. RECIPIENT'S CATALOG NUMBER	
(6) 4. TITLE (and Subtitle): CALCULATIONAL PROCEDURE FOR EVALUATING TIME- AND SPATIAL-DEPENDENT ENERGY DEPOSITION IN AIR FOR ANISOTROPIC NUCLEAR SOURCES; VOL. I, TECHNICAL DISCUSSION (Volume I.)	(9) 5. TYPE OF REPORT & PERIOD COVERED: Technical Report
	6. PERFORMING ORG. REPORT NUMBER: (14) RRA-T7814-I
(10) 7. AUTHOR(s): M. B. Wells and R. B. Livesay	(15) 8. CONTRACT OR GRANT NUMBER(s): F08606-77-C-0008
9. PERFORMING ORGANIZATION NAME AND ADDRESS: RADIATION RESEARCH ASSOCIATES, INC. 3550 Hulen Street Fort Worth, Texas 76107	10. PROGRAM ELEMENT, PROJECT, TASK AREA & WORK UNIT NUMBERS: (12) 76p.
11. CONTROLLING OFFICE NAME AND ADDRESS: AIR FORCE TECHNICAL APPLICATIONS CENTER Patrick Air Force Base, Florida 32925	(11) 12. REPORT DATE: 2 April 1979
	13. NUMBER OF PAGES: 76
14. MONITORING AGENCY NAME & ADDRESS (if different from Controlling Office)	15. SECURITY CLASS. (of this report): Unclassified
	15a. DECLASSIFICATION/DOWNGRADING SCHEDULE

16. DISTRIBUTION STATEMENT (of this Report)

Approved for public release, distribution unlimited

17. DISTRIBUTION STATEMENT (of the abstract entered in Block 20, if different from Report)

18. SUPPLEMENTARY NOTES

19. KEY WORDS (Continue on reverse side if necessary and identify by block number)

Neutron Transport	Monte Carlo Methods
Gamma-Ray Transport	Anisotropic Sources
Secondary Gamma-Ray Transport	Line-Beam Sources

20. ABSTRACT (Continue on reverse side if necessary and identify by block number)

This report describes the RENDER calculational procedure that was developed for use in evaluating the spatial- and time-dependent energy deposition in air produced by anisotropic nuclear sources. The RENDER procedure utilizes nuclear energy deposition data generated for conical sources that were originally computed for line-beam sources through use of the ZAP, ZAPN, ZAPGAM and DEPO codes. The energy deposition data for air that are input to RENDER were generated for neutron and gamma-ray sources and for secondary gamma rays re-

→ next page JOB

DD FORM 1473 EDITION OF 1 NOV 65 IS OBSOLETE

UNCLASSIFIED

SECURITY CLASSIFICATION OF THIS PAGE (When Data Entered)

294 300

sulting from neutron capture and inelastic scattering in air. The energy deposition data for line-beam sources and for point isotropic sources were found to compare favorably with similar data reported in the literature. The RENDER procedure was run utilizing energy deposition data from the conical source-data base for a 9-to-10-MeV gamma-ray source and the results of the convolution over source emission direction and time were found to be in good agreement with the input data, indicating that the RENDER procedure performs the time-and-angle convolution correctly.

Volumes II through IV of this report present tabulated data on the time dependent energy deposition in air versus range for neutron and gamma-ray point isotropic sources and for secondary gamma rays generated by point isotropic neutron sources. Also given in Vol. V are curve fit coefficients for use in computing the energy deposition in air versus distance and source emission angle for line beam sources of neutrons and gamma rays. Coefficient data are also given for secondary gamma-ray energy deposition by line beam neutron sources.

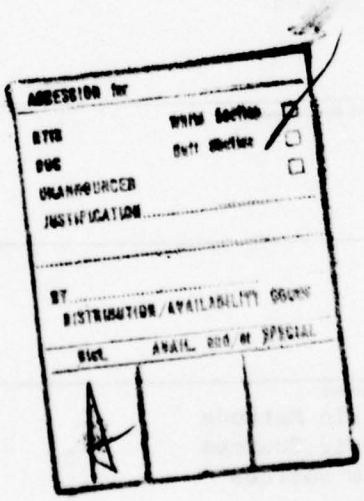

TABLE OF CONTENTS

LIST OF FIGURES

LIST OF FIGURES (Continued)

LIST OF TABLES

LIST OF TABLES (Continued)

I. INTRODUCTION

The studies described in this report were performed for the purpose of providing a calculational procedure for predicting the time and spatial dependency of the nuclear energy deposition (neutron, gamma ray, and neutron-produced secondary gamma rays) in an infinite homogeneous medium of air for anisotropic nuclear sources. There were no data available in the literature at the time this study was started that would provide the needed source energy, time- and spatial-dependent nuclear-energy deposition data for use in the calculational procedure.

The time- and spatial-dependent nuclear-energy deposition calculations were performed as a function of source energy first for line-beam neutron and gamma-ray sources and the resulting data were then converted to give energy deposition data for conical sources. A computer procedure, RENDER, was developed to use the energy deposition data for conical sources to calculate the source energy, time- and spatial-dependent energy depositions resulting from anisotropic nuclear sources.

The atmosphere was assumed to be a homogeneous mixture of nitrogen and oxygen with a density of 1.225 grams per liter. The nuclear cross sections used in the calcualtions are described in Section II. The nuclear energy deposition calculations were performed using the ZAP, ZAPN and ZAPGAM Monte Carlo procedures and the DEPO code (Refs. 1, 2, 3, and 4). A discussion of the calculational methods and the results obtained for line-beam gamma-ray and neutron sources and the secondary gamma-ray sources resulting from gamma-ray production by neutron inelastic scattering and n,γ reactions are also given in Section II.

The time-independent energy-deposition results obtained with these codes were compared with published data to assess the accuracy of the newly-calculated data. The results of these comparisons are given in Section II.

The collision data generated for line-beam sources with use of the ZAP, ZAPN and ZAPGAM Monte Carlo procedures were stored on history tapes.

These history tapes were then used as input to a modified version of the DEPO procedure to generate time- and spatial-dependent energy-deposition data for conical neutron and gamma-ray sources. The calculational methods used are discussed in Section III.

A computer procedure, designated as RENDER, was written to convolute the time- and spatial-dependent energy-deposition data for conical sources with time- and angle-dependent source data for anisotropic nuclear sources. The RENDER procedure is described in Section IV. Some results of RENDER calculations that were run to check out the accuracy of the calculational methods used in the RENDER code are also described in Section IV.

Of special interest to laboratories working on problems related to the exposure of personnel and equipment to nuclear radiation is 1) the time-dependent energy-deposition data for air vs range for point-isotropic sources; 2) the time-integrated energy-deposition data for air vs range for point-isotropic sources; and 3) the time-integrated energy-deposition data for air vs range and source polar angle for line-beam sources. Tables containing these data for neutron, gamma-ray and secondary gamma-ray sources for each of the neutron and gamma-ray source energy intervals considered in this study are given in Vols. II through V of this report.

II. ENERGY DEPOSITION CALCULATIONS FOR LINE-BEAM SOURCES

For the gamma-ray transport calculations, the atmosphere was considered to be a homogeneous mixture of nitrogen, oxygen, helium and argon with number densities of $3.978X10^{19}$, $1.067X10^{19}$, $1.335X10^{14}$ and $2.380X10^{12}$, respectively. The density of the atmosphere was assumed to be 1.225 grams/liter.

The cross section data for air used in the ZAP and ZAPGAM calculations for the total cross section, the photoelectric cross section, the pair production cross section, the coherent scattering cross section and the incoherent scattering cross section as a function of energy were taken from Ref. 5 for 67 energies between 0.1 keV and 100 MeV. The coherent and incoherent scattering structure factors given in Ref. 5 for 45 values of the momentum transfer between 0.0 and $4.85X10^{6}$ ($M_e c$ units) were also used in the gamma-ray scattering calculations.

Neutron cross section data needed for input to ZAPN were generated from ENDF/B -III files (Ref. 6) for nitrogen and oxygen with use of the SAM-X and CBAND procedures (Ref. 7). The ENDF/B files were first employed as input to SAM-X which extracted basic cross section data from the ENDF/B-III files for nitrogen and oxygen and organized the data into the formats required by CBAND. The output from SAM-X is a binary tape (element data tape, ETD) which was then input to CBAND which organized the cross section data into energy bands. The output of CBAND is a magnetic tape which is referred to as an organized data tape (ODT). It is the organized data tape that is used as input to ZAPN.

For the neutron transport problems it was assumed that air was 78% nitrogen and 22% oxygen by volume and the air density was taken to be 1.225 grams/liter.

In ZAPN the inelastic scattering cross section is considered to be the sum of all interactions that produce an x-particle (alpha, protons, gammas, etc.) in addition to inelastically scattering the incident neutron. For nitrogen, the inelastic scattering cross section at energies above

8 MeV is the sum of the (n,n'p), (n,n'γ) and (n,n'α) cross sections and thus not all of the energy required to excite the nucleous to a level or into the continuum (the Q value) goes into the production of gamma rays. ZAPN was modified so that when an inelastic collision occurred with a nitrogen atom, a random number was used to determine if the Q value was to be given off in the form of gamma rays or if charged-particle emission occurs. If $\sigma_{n,n'\gamma}(E)$ is the inelastic scattering cross section for the "x" particles being gamma rays and $\sigma_{n,n'}(E)$ is the total inelastic scattering cross section, then

$$P(E) = \frac{\sigma_{n,n'\gamma}(E)}{\sigma_{n,n'}(E)}$$

is the fraction of the inelastic collisions for which gamma rays are emitted that carry an energy equal to the Q value and (1 - P(E)) is the fraction of the inelastic collisions for which an energy equal to the Q value is carried off by charged particles, such as alpha particles and protons. When an inelastic scattering event was selected to be a non-gamma-ray-producing event, then an energy equal to the Q value was added to the counter denoting the energy deposited by absorption processes. For nitrogen, P(E) was calculated from ENDF/B-III cross sections. Table I lists these values for neutron energies between 8 and 16 MeV. Linear interpolation was used on the data in Table I to obtain values of P(E) at energies between the tabulated energies.

The neutron history tape generated with the ZAPN procedure was used in the SGSORC procedure (Ref. 8) to generate secondary gamma-ray photon sources. The number of gamma rays produced per neutron collision as a function of neutron energy and the energy distribution of the emitted gamma rays as a function of the incident neutron energy were obtained from the ENDF/B-III files for use in the SGSORC procedure.

TABLE I. FRACTION OF THE NONELASTIC COLLISIONS WITH NITROGEN THAT RESULT IN GAMMA-RAY EMISSION

NEUTRON ENERGY (MeV)	$P(E) = \frac{\sigma_{n,n',\gamma(E)}}{\sigma_{n,n'}}$
8.00	1.000
8.50	0.974
9.00	0.900
9.50	0.816
9.75	0.764
10.00	0.708
10.25	0.678
10.05	0.655
10.75	0.629
11.00	0.604
11.25	0.571
11.50	0.543
11.75	0.517
12.00	0.496
12.25	0.477
12.50	0.456
13.00	0.430
13.50	0.414
14.00	0.403
14.50	0.395
15.00	0.387
15.50	0.378
16.00	0.360

For the ZAPGAM calculation of the energy deposition by secondary gamma rays, the same gamma-ray cross-section data used in the ZAP calculations were also used in ZAPGAM.

The geometry used in the energy deposition calculations for line-beam sources is shown in Fig. 1. The source radiation (neutron or gamma ray) is emitted from the source point in the direction $\theta=0°$. The energy deposition was determined for regions formed by the intersection of the conical surfaces generated by the revolution of the radii R_{i-1} and R_i inclined at polar angles θ_{j-1} and θ_j, respectively, about the source axis and the spherical surfaces formed by the revolution of the radii R_{i-1} and R_i about the source point. The radii and polar angles used to define the energy deposition regions out to 1500 meters are listed in Table II.

Because of the fact that gamma rays travel at the speed of light whereas neutrons travel at a speed determined by their energies, different time intervals were used to record the time-dependent energy deposition data for gamma rays, neutrons and secondary gamma rays. Table III lists the time-interval bounds used for each of the three different radiation sources.

The source energy intervals used for the neutron and gamma-ray line-beam sources are listed in Table IV. For the line-beam gamma-ray problems, 10,000 histories were run for each source energy interval and histories were terminated either by a minimum weight cutoff of $1.0X10^{-3}$ or when the number of collisions per history exceeded 30. For the line-beam neutron problems, 2000 histories were run for each source energy interval. Neutron histories were terminated when the number of collisions per history exceeded 200, when the energy reduced below $1.01X10^{-3}$ keV or when the transport time exceeded 1.0 second. The secondary gamma-ray histories were terminated when the number of collisions exceeded 30, when the particle weight reduced by a factor of $1X10^{-3}$ or when the gamma-ray energy had reduced below 0.2 keV. Secondary gamma-ray sources were generated by SGSORC using 10 per cent of the collision data from the first 1000 of the neutron histories stored on the ZAPN-generated collision tapes.

CONICAL SOURCE GEOMETRY

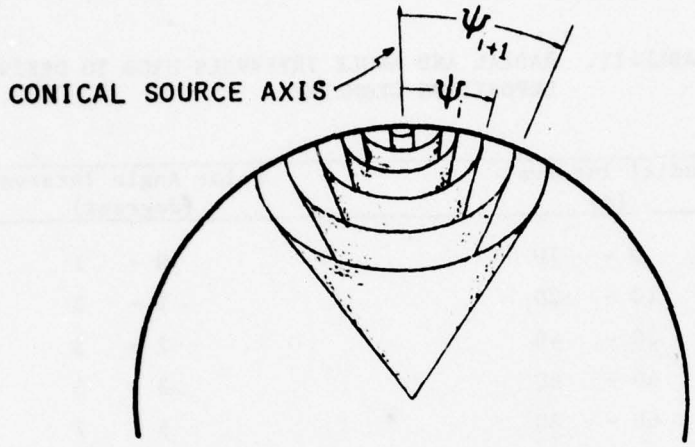

ENERGY DEPOSITION GEOMETRY

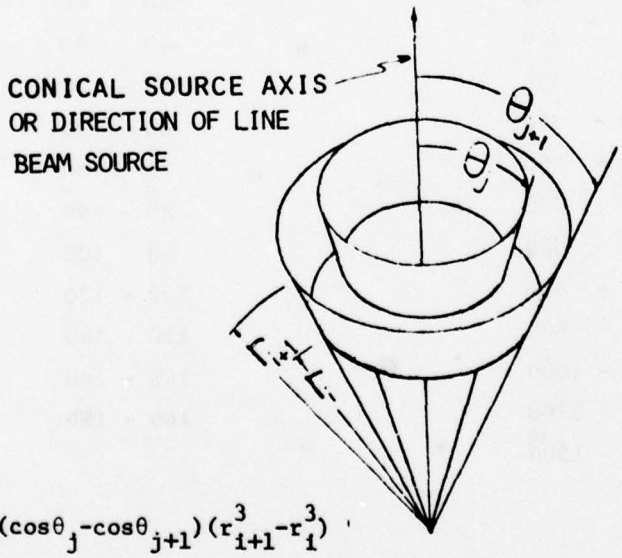

$$dV = \frac{2\pi}{3}(\cos\theta_j - \cos\theta_{j+1})(r_{i+1}^3 - r_i^3)$$

Fig. 1. Energy Deposition Geometry for Line Beam and Conical Sources and Source Geometry for Conical Sources

TABLE II. RADIAL AND ANGLE INTERVALS USED TO DEFINE DEPOSITION GEOMETRY

Radial Interval (m)	Polar Angle Interval (degrees)
0 - 10	0 - 1
10 - 20	1 - 2
20 - 40	2 - 3
40 - 60	3 - 5
60 - 80	5 - 7
80 - 100	7 - 10
100 - 125	10 - 15
125 - 150	15 - 20
150 - 175	20 - 30
175 - 200	30 - 40
200 - 250	40 - 50
250 - 300	50 - 60
300 - 350	60 - 70
350 - 400	70 - 80
400 - 450	80 - 90
450 - 500	90 - 100
500 - 600	100 - 120
600 - 800	120 - 140
800 - 1000	140 - 160
1000 - 1200	160 - 180
1200 - 1500	

TABLE III. BOUNDS OF DEPOSITION TIME INTERVALS USED IN NEUTRON, SECONDARY GAMMA-RAY AND PRIMARY GAMMA-RAY PROBLEMS

DEPOSITION TIME INTERVAL (μsec)	
Neutrons and Secondary Gamma-Ray Problems	Primary Gamma Problems
0 - 0.2	$0 - 10^{-14}$
0.2 - 0.3	$10^{-14} - 0.02$
0.3 - 0.5	0.02 - 0.05
0.5 - 1.0	0.05 - 0.07
1 - 2	0.07 - 0.10
2 - 3	0.10 - 0.15
3 - 5	0.15 - 0.20
5 - 7	0.20 - 0.30
7 - 10	0.30 - 0.50
10 - 20	0.50 - 0.70
20 - 35	0.70 - 1.00
35 - 50	1.00 - 1.50
50 - 70	1.50 - 2.00
70 - 100	2.00 - 3.00
100 - 200	3.00 - 5.00
200 - 400	5.00 - 7.00
400 - 700	7.00 - 10.00
700 - 1000	
1000 - 2000	
2000 - 3500	
3500 - 15000	
15000 - 100,000	

TABLE IV. SOURCE ENERGY INTERVAL BOUNDS USED FOR NEUTRON AND PRIMARY GAMMA-RAY PROBLEMS

Neutron Source Energy Intervals (MeV)	Primary Gamma-Ray Energy Intervals (MeV)
0.001 - 0.00335	9.0 - 10.0
0.00335 - 0.0912	8.0 - 9.0
0.0912 - 0.0248	7.0 - 8.0
0.0248 - 0.0676	6.0 - 7.0
0.0676 - 0.184	5.0 - 6.0
0.184 - 0.303	4.0 - 5.0
0.303 - 0.50	3.0 - 4.0
0.50 - 0.823	2.0 - 3.0
0.823 - 1.353	1.0 - 2.0
1.353 - 1.738	0.5 - 1.0
1.738 - 2.232	0.1 - 0.5
2.232 - 2.865	0.01 - 0.1
2.865 - 3.680	
3.680 - 6.070	
6.070 - 7.790	
7.790 - 10.0	
10.0 - 12.0	
12.0 - 13.5	
13.5 - 15.0	

The line-beam source problems were run using the computer code outlined in Fig. 2. The ZAPXG procedure was used to generate collision data for line-beam gamma-ray sources. The ZAPNO1 procedure was used to generate collision data for line-beam neutron sources. The collision data generated by the line-beam neutron and gamma-ray problems were stored on magenetic tapes (history tapes). The collision data on the neutron history tapes were rearranged with use of the RETAPE code so that the resulting neutron history tapes could be read by both the SGSRO1 procedure and the DEPO procedure. The SGSRO1 procedure was used with the neutron history tapes to generate secondary gamma-ray source data for input to the ZAPGAM procedure which was then used to generate secondary gamma-ray history tapes. The DEPO procedure was used to read the history tapes generated by each of the ZAPXG, ZAPNO1 and ZAPGAM runs and to calculate the energy deposition occurring within the energy deposition volumes and deposition time intervals given in Tables II and III. The output of the DEPO runs were obtained in both printed and computer tape formats. For each ZAP, ZAPN and ZAPGAM problem run, the DEPO printed output gave 3 pages of printout (energy deposition vs radial interval and polar angle interval) for each source time interval and each source energy interval and a final 3 pages for the time-integrated data for each source energy interval. This resulted in 648 pages of output for the primary gamma-ray problems, 1197 pages of output for the neutron problems and 1311 pages output for the secondary gamma-ray problems.

The printed output from the DEPO procedure and the Monte Carlo runs were examined to insure that no energy was lost in the Monte Carlo calculations. Table V lists the fraction of the primary gamma-ray source energy that was deposited in the atmosphere within 1500 meters slant range by gamma-ray scattering and absorption interactions. The difference between 1 and the fraction of the source energy deposited in the atmosphere is the fraction of the source energy that was lost due to the use of Russian Roulette in terminating histories by minimum weight cutoff, by photons that underwent more than 30 collisions per history and by photons that

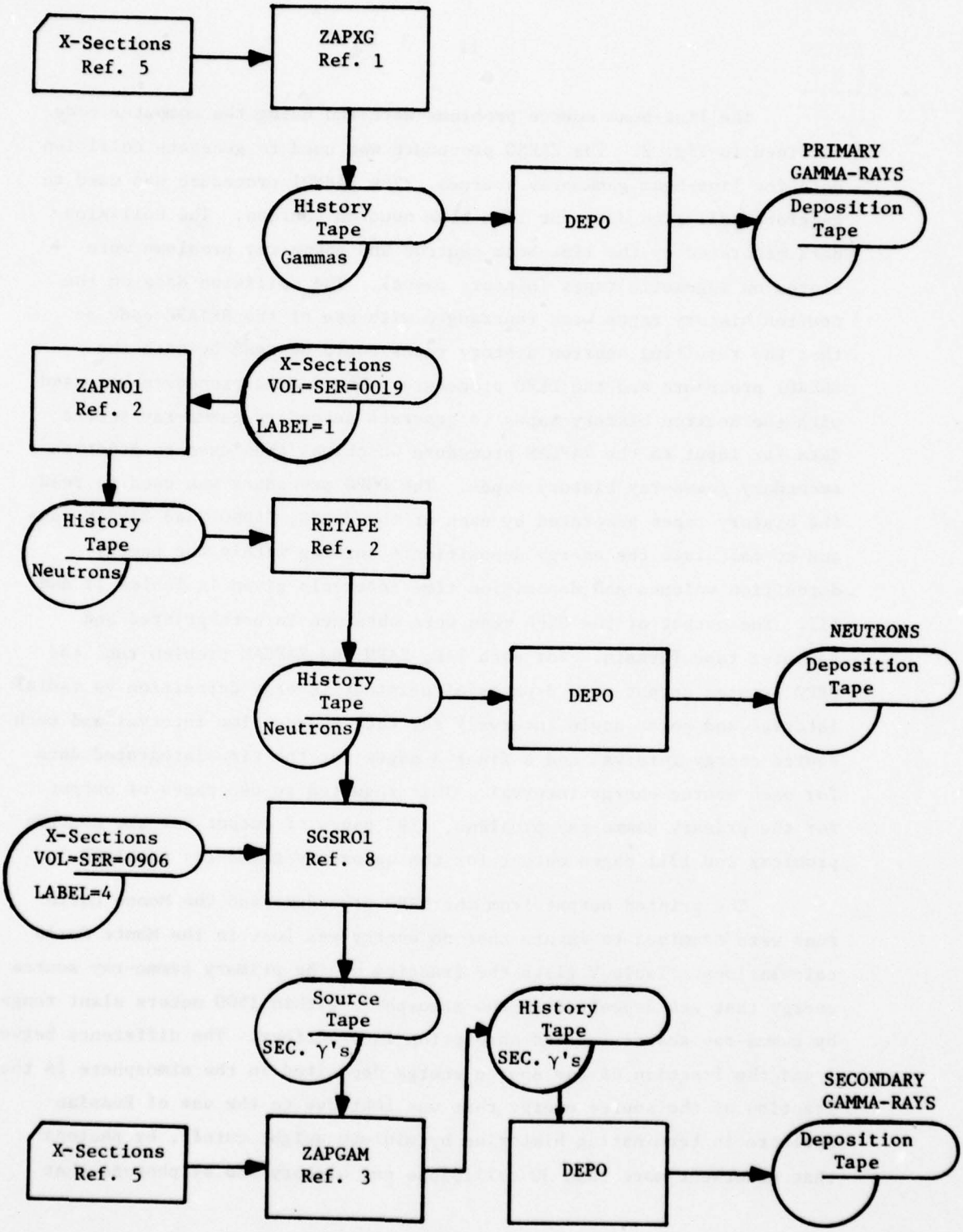

Fig. 2. Calculation Flow for Energy Deposition Calculations

TABLE V. ENERGY DEPOSITED FOR SLANT RANGES LESS THAN 1500 METERS AND AVERAGE NUMBER OF COLLISIONS PER HISTORY FOR GAMMA-RAY SOURCES

Gamma-Ray Source Energy Interval (MeV)	Fraction of Source Energy Deposited by Scattering and Absorption (MeV)	Average Number of Collisions per History
0.01-0.1	0.9697	13.0
0.1-0.5	0.9916	22.6
0.5-1.0	0.9971	24.4
1.0-2.0	0.9965	25.1
2.0-3.0	0.9928	25.4
3.0-4.0	0.9890	25.5
4.0-5.0	0.9846	25.6
5.0-6.0	0.9788	25.7
6.0-7.0	0.9711	25.8
7.0-8.0	0.9613	25.8
8.0-9.0	0.9593	25.8
9.0-10	0.9570	25.8

deposited energy at slant ranges greater than 1500 meters. It is seen that 4.3 per cent or less of the source energy was not deposited by scattering or absorption interactions within 1500 meters slant range. Although the maximum number of collisions allowed per history was 30, the number actually undergone was less than 30. The average number of collisions required per history was approximately 26 for source energies above 1.0 MeV and reduced to 13 for source energies between 0.01 and 0.1 MeV.

The neutron energy deposited in the atmosphere out to 1500 meters radius about the source point is shown in Table VI. Also shown is the Q value for neutrons with energies above 2.232 MeV. The sum of the energy deposited and the Q value is also shown in the table. The difference between the average source energy and this sum represents the neutron energy lost by neutrons at slant ranges greater than 1500 meters and by the various history termination methods. Table VI shows that no energy was lost in the neutron transport calculations. The average number of collisions per history for the neutron problems varied with the source energy, with 167 required for an average source energy of 6.93 MeV to 107 for an average source energy of 0.002175 MeV.

The secondary gamma-ray energy generated per source neutron by the SGSC procedure is given as a function of the neutron source energy interval in Table VII. Also tabulated is the secondary gamma-ray energy deposited within a slant range of 1500 meters. Only 10 per cent of the neutron collisions generated by the first 1000 neutron histories was used in generating secondary gamma-ray photons. An adjustment in the weight of the secondary gamma-ray source photons started was used to correct for the bias sampling. The average number of secondary gamma-ray photon histories traced is also listed in Table VII for each neutron source energy interval. On the average, it took approximately 25.6 collisions per secondary gamma-ray history to deposit all of the gamma-ray energy. This is approximately the same number of collisions per history required for primary gamma rays with source energies above 2.0 MeV (see Table V).

TABLE VI. NEUTRON ENERGY DEPOSITED BY SCATTERING AND ABSORPTION, Q VALUE AND AVERAGE NUMBER OF NEUTRON COLLISIONS PER HISTORY

Average Source Energy (MeV)	Energy Deposited by Scattering and absorption	Q Value	Energy Deposited Plus Q Value	Average No. of collisions/history
.002175	.002172		.002172	107
.006235	.006281		.006281	115
.01696	.0168		.0168	122
.0462	.04607		.04607	130
.1258	.0258		.0258	138
.2435	.2425		.2425	142
.4015	.3997		.3997	146
.6615	.6610		.6610	150
1.088	1.089		1.089	154
1.568	1.546		1.546	157
2.0075	1.987		1.987	159
2.5485	2.538	.00282	2.541	161
3.2725	3.250	.00762	3.258	163
4.8750	4.694	.1726	4.867	165
6.930	5.832	1.108	6.940	167
8.895	6.824	2.063	8.887	166
11.000	8.390	2.612	11.00	165
12.75	9.936	2.819	12.76	165
14.25	11.00	3.270	14.27	165

TABLE. VII. SECONDARY GAMMA ENERGY GENERATED IN SGSC AND DEPOSITED IN ZAPGAM-DEPO CALCULATIONS, AVERAGE NUMBER OF COLLISIONS PER HISTORY AND NUMBER OF SECONDARY GAMMA-RAY HISTORIES

Neutron Source Energy Interval (MeV)	Secondary Gamma Energy Generated by SGSC per Source Neutron (MeV)	Secondary Gamma Energy Deposited by ZAPGAM-DEPO (MeV)	Average No. of Collisions per History	Number of Secondary Gamma Histories
.001 - .00335	.437	.4359	25.56	14,158
.00335- .00912	.4404	.4503	25.56	14,250
.00912- .0248	.4409	.4358	25.57	14,071
.0248 - .0676	.4516	.4429	25.56	14,372
.0676 - .184	.4516	.4464	25.59	14,307
.184 - .303	.4364	.4277	25.58	14,107
.303 - .5	.4297	.4424	25.59	14,117
.5 - .823	.4198	.4114	25.62	14,308
.823 - 1.353	.4098	.3996	25.58	14,243
1.353 - 1.783	.3634	.3589	25.53	14,280
1.783 - 2.232	.362	.3369	25.59	14,589
2.232 - 2.865	.2824	.2755	25.59	14,511
2.865 - 3.680	.2342	.2344	25.54	14,884
3.680 - 6.07	.3867	.3829	25.52	15,432
6.07 - 7.79	1.412	1.437	25.58	15,805
7.79 -10.0	2.851	2.758	25.54	15,964
10.0 -12.0	3.561	3.602	25.53	16,229
12.0 -13.5	3.460	3.461	25.54	16,189
13.5 - 15.0	3.417	3.310	25.54	16,384

Wells (Ref. 9) has published the results of Monte Carlo calculations of the gamma-ray dose rate in an infinite air medium for point monodirectional sources at source energies of 0.6, 1.0, 3.0, and 6.2 MeV and for source-receiver distances between 500 and 3750 ft. Zerby et al. (Ref. 10) have also published similar data for source-receiver distances of 5, 10, 20, 40, 65 and 100 ft. The gamma-ray air-scattering data from these two separate calculations have been incorporated as library data in the SKYSHINE Monte Carlo procedure (Ref. 11) for use in evaluating the gamma-ray exposure in air for personnel in the vicinity of the turbine building of a nuclear power plant. The SKYSHINE library data were transformed to the air density used in the ZAP calculations (ρ=1.225X10^{-3} g/cm^3) for comparison with the ZAP energy deposition data. Figures 3 and 4 show a comparison of the ZAP calculations for 6-7 MeV gamma rays at 161 meters and 884 meters with the SKYSHINE data for 6.2 MeV gamma rays. The agreement between the calculations is good, considering the differences in the source energies.

The integral of the ZAP-DEPO calculations for line-beam sources over the source polar angle θ and the azimuthal angle ϕ (see Fig. 1) for given source-receiver distances gives the energy deposition versus source-receiver distance for a point isotropic source. If $ED(E_o,\theta,R)$ is the energy deposited per unit volume at position θ,R for source energy E_o, then

$$ED(E_o,R) = \int_0^{2\pi}\int_0^{\pi} \frac{1}{4\pi} ED(E_o,\theta,R) \sin\theta d\theta d\theta$$

is the energy deposited per unit volume at position R for an isotropic source emitting 1 photon in all directions. Clark (Ref. 12) has published the results of moments method calculations of gamma-ray energy deposition in air. His results were reported in the form of energy build-up factors for a number of gamma-ray energies. He expressed the build-up factor with use of the equation

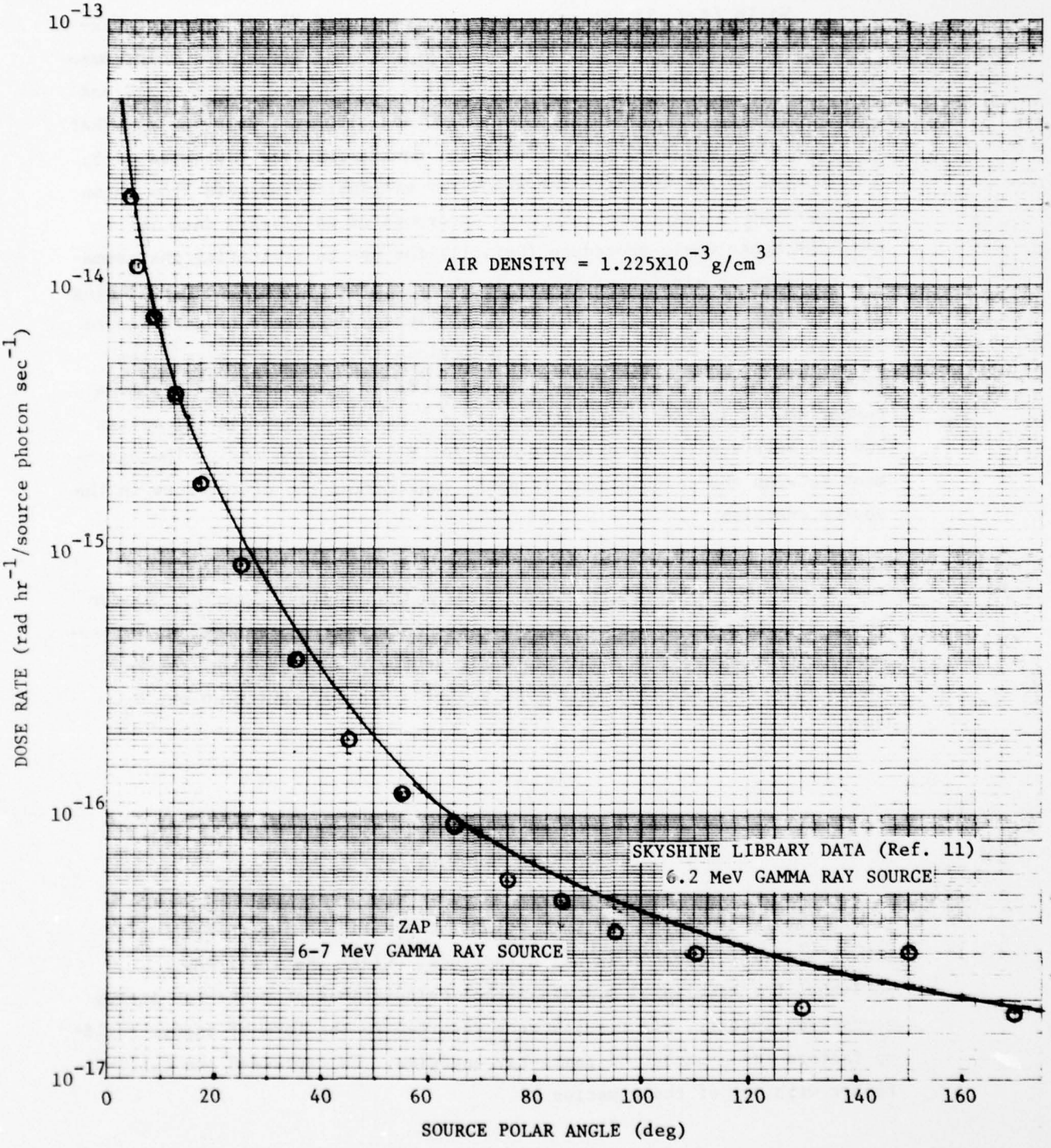

Fig. 3. Comparison of ZAP Calculations of the Gamma Ray Dose Rate in Air at 161 Meters with Data from SKYSHINE Library

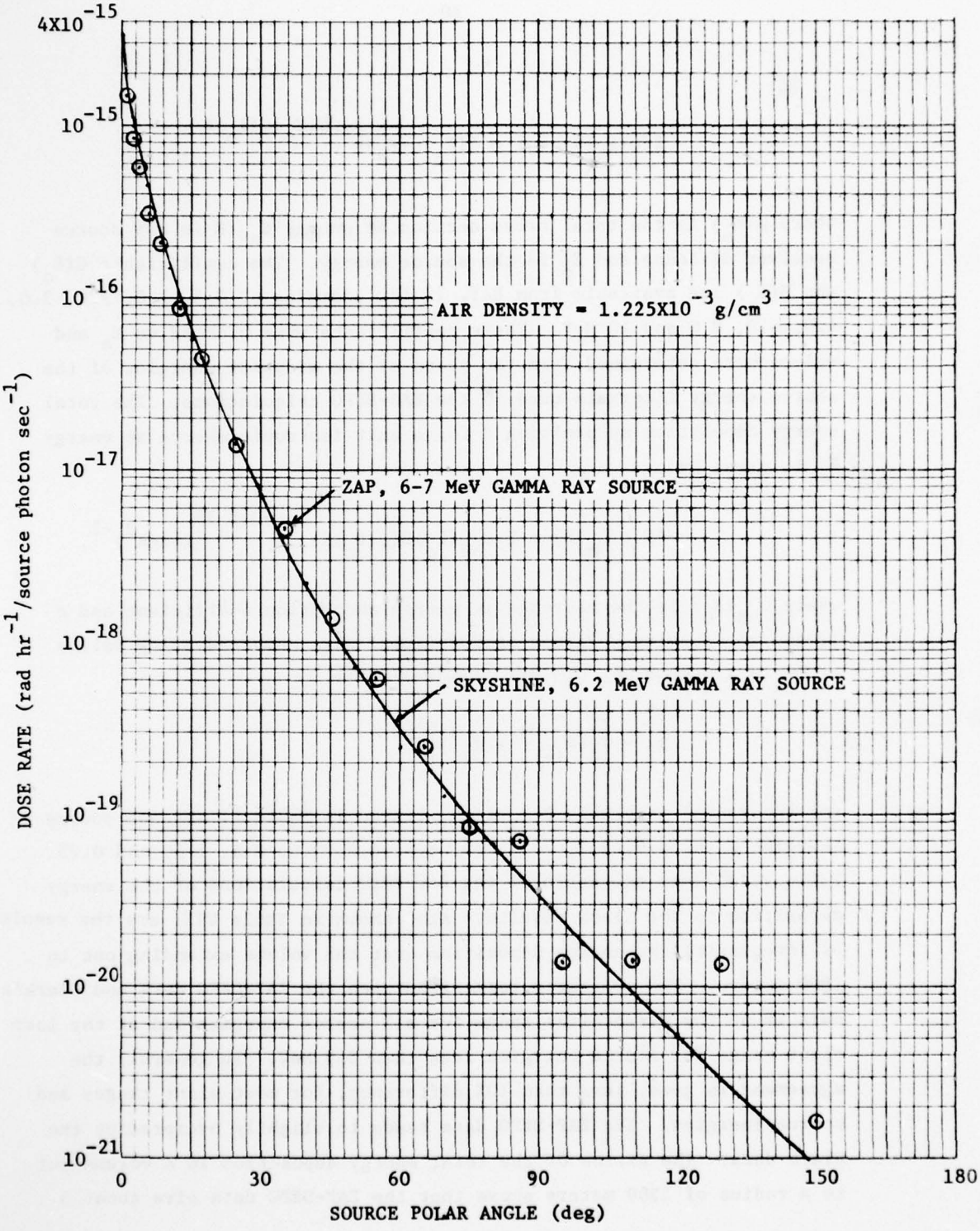

Fig. 4. Comparison of ZAP Calculations of the Gamma-Ray Dose Rate in Air at 884 Meters with Data from SKYSHINE Library

$$B(\mu(E_o)R) = 1 + C(E_o)\mu(E_o)R\, e^{D(E_o)\mu(E_o)R},$$

where $\mu(E_o)$ is the total cross section at energy E_o, R is the source receiver distance and E_o is the source energy. The coefficients $C(E_o)$ and $D(E_o)$ are available from Ref. 12 for energies of 0.5, 1.0, 2.0, 3.0, 4.0, 6.0, 8.0 and 10 MeV. These coefficients were plotted vs E_o and values were determined from the plots at the midpoint energies of the source energy intervals used in the ZAP-DEPO calculations. The total energy deposition at position R for a unit isotropic source at energy E_o is given by

$$ED(\mu(E_o)R) = E_o\mu_{ea}(E_o)B(\mu(E_o)R)\; e^{-\mu(E_o)R}(4\pi\rho R^2)^{-1},$$

where $\mu_{ea}(E_o)$ is the macroscopic energy absorption coefficient and ρ is the air density. Values of $ED(\mu(E_o)R)$ were computed using values of $\mu_{ea}(e_o)/\rho$ from Ref. 13 and $\bar{R}$ values given by

$$\bar{R}_i = \left[\frac{1}{2}(R_{i-1}^3 + R_i^3)\right]^{1/3}$$

for the radial intervals R_{i-1} to R_i listed in Table II and and source energies E_o of 4.5, 8.5, 7.5, 6.5, 5.5, 4.5, 3.5, 2.5, 1.5, and 0.75. Table VIII lists the ratio of the ZAP-DEPO calculations of the energy deposition to the Clark results. Also shown in Table VIII are the results of integrating the energy deposition over the volume extending out to 1500 meters. The poorest agreement between the ZAP-DEPO data and Clark's data is at the first slant range for all source energies and at the last slant range for source energies less than 3.5 MeV. In general, the agreement is good, less than 10% difference, for most slant ranges and source energies. The ZAP-DEPO data tends to slightly overpredict the Clark data. The ratios of the total energy deposition in a volume out to a radius of 1500 meters shows that the ZAP-DEPO data give about 5

TABLE VIII. RATIO OF THE GAMMA-RAY ENERGY DEPOSITION PER UNIT VOLUME OF AIR FROM A POINT ISOTROPIC SOURCE AS COMPUTED WITH ZAP-DEPO TO THAT COMPUTED USING CLARK'S ENERGY BUILDUP FACTOR DATA VERSUS SOURCE ENERGY AND SLANT RANGE

	SOURCE ENERGY (MeV)									
R(cm)	0.75	1.5	2.5	3.5	4.5	5.5	6.5	7.5	8.5	9.5
7.937+2*	1.885	1.967	1.823	1.929	1.817	1.949	1.889	1.902	1.831	2.090
1.651+3	1.081	1.154	1.151	1.111	1.033	1.230	1.167	1.123	1.037	1.260
3.302+3	1.088	1.165	1.146	1.173	1.160	1.185	1.195	1.171	1.180	1.231
5.192+3	1.035	1.048	1.072	1.034	1.049	1.063	1.060	1.055	1.143	1.131
7.140+3	0.938	1.035	1.112	1.055	1.038	1.103	1.147	1.004	0.984	1.140
9.110+3	0.946	0.939	0.997	1.024	1.061	1.006	1.038	1.017	1.010	1.031
1.139+4	0.976	0.972	0.971	0.949	0.974	1.056	1.070	1.085	1.089	1.087
1.386+4	0.985	0.977	0.995	1.064	1.075	1.072	1.025	0.971	1.117	1.028
1.635+4	0.996	0.985	0.955	1.092	1.042	1.036	0.981	1.088	1.068	1.075
1.883+4	0.987	0.993	1.020	1.106	1.106	1.054	0.980	1.030	1.069	1.049
2.277+4	1.002	1.040	1.051	1.056	1.048	0.986	1.071	1.088	1.071	1.017
2.773+4	1.061	1.021	1.012	1.001	0.780	1.089	1.024	1.073	1.056	1.082
3.269+4	1.142	1.095	1.067	1.053	1.042	0.994	1.010	1.072	1.081	1.042
3.767+4	1.133	1.051	1.030	1.005	1.020	1.018	0.953	1.000	1.058	1.038
4.265+4	1.205	1.034	1.079	1.057	1.077	1.019	1.017	1.039	0.989	0.979
4.763+4	1.286	1.043	1.057	1.076	1.114	1.142	1.088	1.016	1.022	1.043
5.545+4	1.354	1.092	1.118	1.112	1.079	1.062	1.028	1.045	1.004	1.027
7.140+4	1.548	1.271	1.279	1.143	1.108	1.075	1.115	1.071	1.011	1.044
9.110+4	1.375	1.208	1.163	1.086	1.080	1.005	1.059	1.044	0.993	0.968
1.109+5	1.166	1.199	1.125	1.077	1.048	1.047	1.114	0.932	1.026	0.939
1.366+5	2.487	1.588	1.477	1.174	1.039	1.130	1.028	1.063	1.095	0.933
0-1.5+5	1.070	1.066	1.082	1.078	1.073	1.068	1.066	1.092	1.056	1.053

*Read 7.937+2 as 7.937×10^2

to 8% more energy deposition than do the Clark data.

There does not appear to have been any previous calculations of the neutron and secondary gamma-ray dose rates in air for line-beam neutron sources other than those reported previously by Wells in Ref. 14. Those calculations were performed in 1960 and the neutron and secondary gamma-ray production cross sections used in those calculations are out of date. In addition, the calculations were not made for source-receiver distances greater than 100 ft. Therefore, the ZAPN-DEPO and ZAPGAM-DEPO calculations for line-beam sources were integrated over the source polar angle to provide data for comparison with calculations for point-isotropic neutron sources. Straker (Ref. 15) has reported the results of his calculations of the neutron dose (air kerma) in an infinite homogeneous air medium for a 12.2-15 MeV point-isotropic neutron source. Straker's data, in units of $4\pi R^2$ times the neutron dose (cm^2 Rad/source neutron), are compared in Fig. 5 with the results given by the ZAPN-DEPO calculations for a neutron source emitting uniformly between 12.0 MeV and 15 MeV. The dose rates computed by ZAPN-DEPO for an air density of 1.225×10^{-3} g/cm^3 were transformed to an air density of 1.11×10^{-3} g/cm^3, which was the air density used in Straker's calculations. The comparison in Fig. 5 shows that the ZAPN-DEPO calculations slightly overpredict Straker's calculations as a function of slant range by about 10 $\sim$ 15% over most of the slant range considered. Considering the possible differences in the neutron cross sections used in the two different calculations, the agreement between the calculations is good.

Straker (Ref. 15) has also reported the results of calculations of the secondary gamma-ray dose in an infinite homogeneous air medium that results from the atmospheric absorption and scattering of neutrons that were emitted by a 12.2 MeV to 15 MeV point-isotropic source. His results are compared in Fig. 6 with similar results from the ZAPGAM-DEPO calculations for a 12.2 to 15 MeV point isotropic neutron source. Straker's calculations were based on the use of Young and Foster's (Ref. 16) evaluation of the neutron cross sections and the secondary gamma-

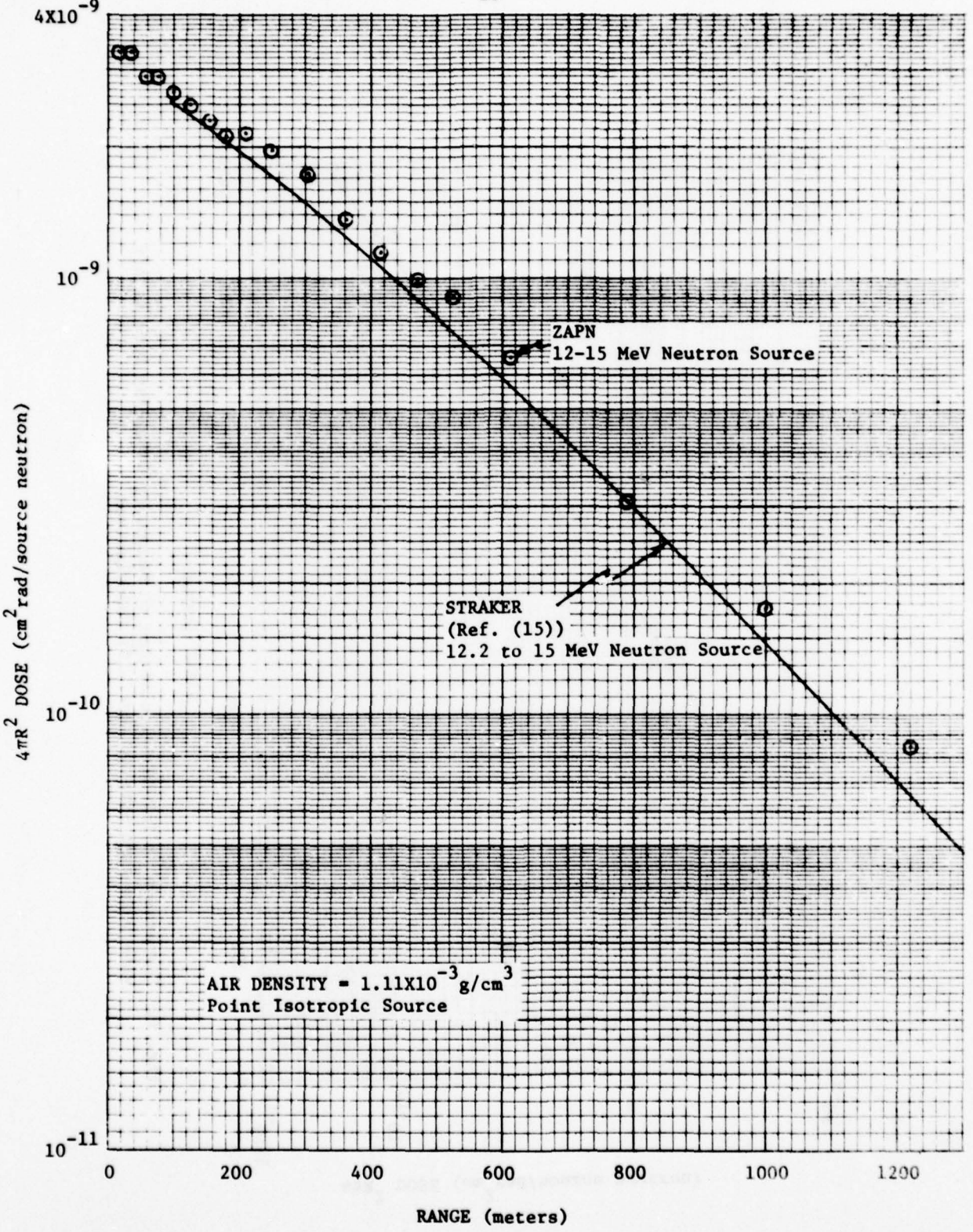

Fig. 5. Comparison of ZAPN Calculations of Neutron Dose in Air with Data from Straker's (Ref. 15) Calculations

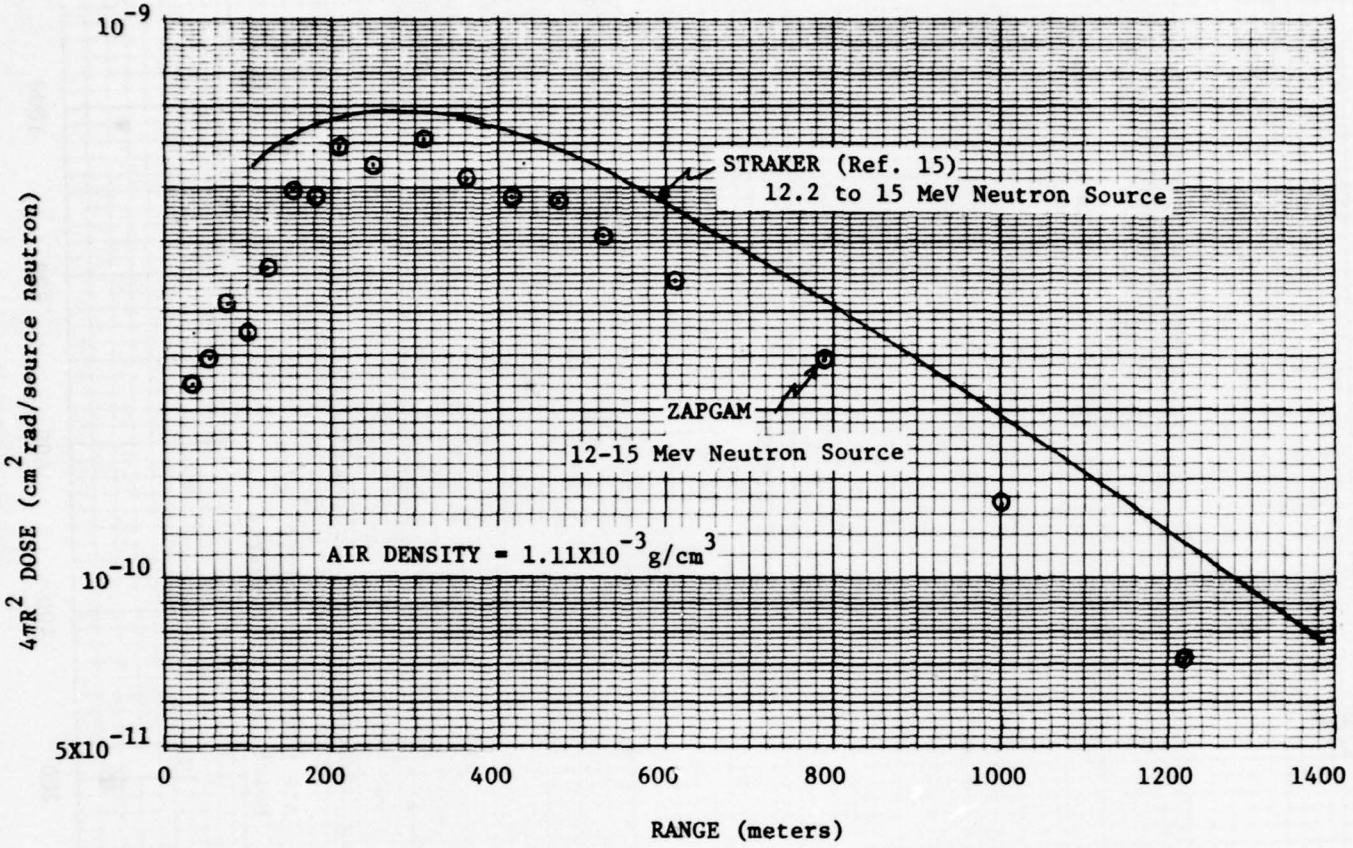

Fig. 6. Comparison of ZAPGAM Calculations of Secondary Gamma-Ray Dose in Air with Data from Straker (Ref. 15) Calculations

ray production cross sections for nitrogen. Young and Foster's evaluation was to later become the basis of the ENDF/B-IV evaluated neutron cross sections for nitrogen. Straker's data are about 35% higher than the ZAPGAM-DEPO data for slant ranges less than 1500 meters. The differences between the two calculations are believed to be due to differences in the secondary gamma-ray production cross sections used in the two calculations.

The DEPO calculations sum the energy deposition at each collision, with the time dependence given in terms of retarded time where retarded time is the actual time at collision minus the time it would take for light to propagate from the source to the collision.

The time dependence of the gamma-ray energy deposited in a sphere of air 1500 meters in radius per keV of source energy for point-isotropic sources emitting within each of the 12 source energy intervals is given in Table IX. The gamma-ray energy deposited in the atmosphere within a retarded time interval of 0 to 10^{-20} seconds represents the energy deposited by first-order scattering and absorption interactions. It is seen that the fraction of the source energy that is absorbed as a result of first-order scattering or absorption events reduces with decreasing source energy until a source energy of 10 keV is reached and then the fraction increases with decreasing source energy. The fraction of the gamma-ray source energy absorbed within a sphere of air with a 1500-meter radius (keV sec^{-1}/keV of source energy times 10^{-20} sec) closely follows the variation of the ratio of the energy absorption to total cross section with energy (see Fig. 7), where the cross section data were taken from Ref. 13. The time dependence of the absorbed gamma radiation for times between 10^{-20} sec and $1X10^{-5}$ sec reduces rapidly with an increase in retarded time. The rate of reduction with increasing retarded time reduces with a decrease in the source energy. At a retarded time of $7X10^{-7}$ sec there is a factor of 10 more energy being deposited by the 10-to-100-keV source than is being deposited by the 9-to-10-keV source.

TABLE IX. TIME DEPENDENT GAMMA-RAY ENERGY DEPOSITION IN SPHERE OF AIR WITH RADIUS OF 1500 METERS

(keV sec^{-1}/keV of source energy)

UPPER BOUND OF TIME INTERVAL(sec)	SOURCE ENERGY INTERVAL											
	10-100 keV	100-500 keV	500 keV -1 MeV	1-2MeV	2-3 MeV	3-4 MeV	4-5 MeV	5-6 MeV	6-7 MeV	7-8 MeV	8-9 MeV	9-10 MeV
10^{-20}	3.033+19	2.495+19	3.779+19	4.594+19	5.172+19	5.559+19	5.893+19	6.161+19	6.273+19	6.366+19	6.573+19	6.679+19
$2X10^{-8}$	5.759+6	5.796+6	7.753+6	8.826+6	9.387+6	9.329+6	9.214+6	8.827+6	8.844+6	8.792+6	8.333+6	8.316+6
$5X10^{-8}$	2.301+6	2.151+6	2.443+6	2.464+6	2.196+6	2.056+6	1.867+6	1.729+6	1.542+6	1.389+6	1.281+6	1.178+6
$7X10^{-8}$	1.711+6	1.520+6	1.486+6	1.369+6	1.296+6	1.161+6	9.290+5	8.220+5	7.707+5	6.542+5	6.335+5	5.378+5
$1X10^{-7}$	1.394+6	1.170+6	1.098+6	1.031+6	8.423+5	7.610+5	6.624+5	5.530+5	5.024+5	4.599+5	4.044+5	3.664+5
$1.5X10^{-7}$	1.137+6	9.472+5	8.080+5	6.605+5	5.710+5	4.850+5	3.996+5	3.537+5	3.064+5	2.832+5	2.430+5	2.183+5
$2.0X10^{-7}$	9.228+5	7.519+5	5.755+5	4.759+5	3.705+5	3.145+5	2.586+5	2.258+5	1.987+5	1.754+5	1.640+5	1.451+5
$3.0X10^{-7}$	7.271+5	5.930+5	4.100+5	3.134+5	2.440+5	1.962+5	1.732+5	1.543+5	1.333+5	1.165+5	1.036+5	9.011+4
$5.0X10^{-7}$	4.723+5	4.306+5	2.695+5	1.802+5	1.381+5	1.118+5	9.342+4	7.987+4	7.221+4	6.423+4	5.671+4	5.396+4
$7.0X10^{-7}$	2.900+5	3.191+5	1.798+5	1.162+5	8.285+4	6.475+4	5.611+4	4.748+4	4.219+4	3.805+4	3.477+4	3.122+4
$1.0X10^{-6}$	1.553+5	2.393+5	1.283+5	7.940+4	5.398+4	4.380+4	3.580+4	3.062+4	2.781+4	2.466+4	2.251+4	2.059+4
$1.5X10^{-6}$	5.091+4	1.496+5	8.528+4	5.091+4	3.420+4	2.644+4	2.168+4	1.884+4	1.716+4	1.516+4	1.406+4	1.290+4
$2.0X10^{-6}$	1.013+4	6.905+4	5.039+4	3.098+4	2.017+4	1.618+4	1.351+4	1.147+4	1.039+4	9.033+3	8.118+3	7.727+3
$3.0X10^{-6}$	8.657+2	1.881+4	1.839+4	1.271+4	9.043+3	7.205+3	6.088+3	5.238+3	4.824+3	4.189+3	3.795+3	3.592+3
$5.0X10^{-6}$	1.326+1	9.954+2	1.690+3	1.526+3	1.308+3	1.123+3	9.901+2	8.439+2	8.332+2	7.372+2	6.809+2	6.279+2
$7.0X10^{-6}$	0	1.515+0	9.036+0	3.467+1	4.334+1	2.788+1	3.726+1	3.174+1	3.794+1	2.839+1	2.990+1	2.772+1
$1.0X10^{-5}$	0	0	0	1.472-2	2.114-1	4.852-1	4.512-1	1.280+0	7.966-1	7.314-1	6.822-1	4.373-1

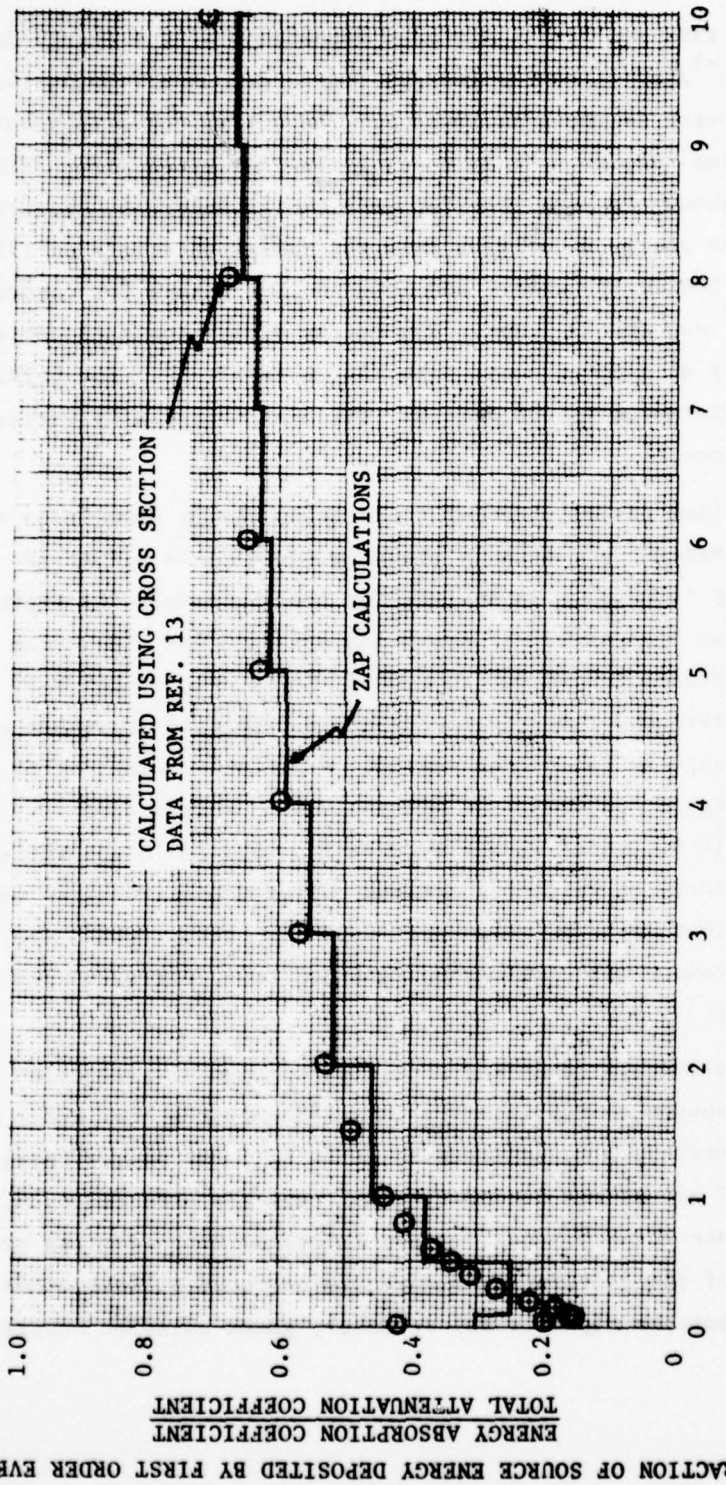

Fig. 7. Fraction of Source Energy Deposited in Air by First Order Scattering and Absorption Events

The time and radial distance dependence of the energy deposition (keV m^{-3} sec^{-1}/keV of source energy) from a 6-to-7-MeV point-isotropic gamma-ray source is shown in Table X. The energy deposition rate in retarded time reduces with increasing time for times after $2X10^{-8}$ seconds at about the same rate for each radial interval. Figure 8 shows a plot of the energy deposition rate for radial intervals of 175 to 200 meters, 500 to 600 meters and 1000 to 1200 meters for retarded times between 10^{-8} sec and 10^{-5} sec. The energy deposition rate varies approximately as a power curve with $ED(t,R)=a(R)t^{-1.33}$ for $t>2X10^{-8}$ sec and radial distances $R\leq1500$ meters. The coefficient a(R) varies with the radial distance.

The time distribution of the neutron energy deposition in a sphere of air 1500 meters in radius is shown in Table XI as a function of the source-energy interval. In the earlier time intervals the energy deposition rate increases by a factor of approximately $2X10^{5}$ as the source energy interval increases from 0.001 to 0.00335 MeV to 13.5 to 15 MeV. With an increase in retarded time the energy deposition rate increases slower with an increase in the source energy. At retarded times after $2X10^{-5}$ sec, the energy deposition rate increases with source energy to a maximum after which it decreases with a further increase in the source energy. The source energy at which the maximum energy deposition rate is found decreases with increasing retarded time. The rate at which the energy deposition reduces with increasing retarded time increases with increasing source energy.

The secondary gamma-ray energy deposition as a function of time and neutron source energy interval in a 1500-meter sphere about a point-isotropic neutron source is given in Table XII. For source energies less than 3.68 MeV all of the secondary gamma rays are produced by n,γ interactions. Since the n,γ cross section increases with reducing neutron energy, all of the capture gamma rays are produced at late times. A significant portion of the total secondary gamma emission occurs in the

TABLE X. TIME-DEPENDENT ENERGY DEPOSITION IN AIR VS RADIAL DISTANCE FROM A POINT ISOTROPIC GAMMA-RAY SOURCE EMITTING UNIFORMLY IN THE ENERGY INTERVAL FROM 6 to 7 MeV

($keV\ m^{-3}\ sec^{-1}$/keV of source energy)

RADIAL DISTANCE INTERVAL (METERS)	DELAY TIME (SEC) .00E 00 - 1.00E-20	1.00E-20 - 2.00E-08	2.00E-08 - 5.00E-08	5.00E-08 - 7.00E-08	7.00E-08 - 1.00E-07	1.00E-07 - 1.50E-07
.0 - 10.0	4.445E 14	9.925E 00	1.718E-01	1.361E-02	2.002E-02	5.645E-03
10.0 - 20.0	6.160E 13	1.786E 00	6.140E-02	2.222E-02	1.098E-03	4.858E-03
20.0 - 40.0	1.449E 13	8.530E-01	1.262E-02	1.140E-02	7.070E-03	3.906E-03
40.0 - 60.0	4.904E 12	3.324E-01	1.247E-02	5.855E-03	4.208E-03	1.671E-03
60.0 - 80.0	2.666E 12	1.978E-01	8.865E-03	3.832E-03	3.127E-03	1.898E-03
80.0 - 100.0	1.427E 12	9.960E-02	5.825E-03	3.190E-03	2.298E-03	1.082E-03
100.0 - 125.0	8.445E 11	8.685E-02	5.055E-03	2.915E-03	1.088E-03	1.100E-03
125.0 - 150.0	4.982E 11	6.080E-02	4.316E-03	1.827E-03	1.355E-03	8.575E-04
150.0 - 175.0	3.269E 11	3.600E-02	3.265E-03	1.898E-03	1.141E-03	6.375E-04
175.0 - 200.0	2.235E 11	2.918E-02	3.311E-03	1.840E-03	7.415E-04	5.180E-04
200.0 - 250.0	1.531E 11	2.056E-02	2.180E-03	1.018E-03	6.250E-04	4.941E-04
250.0 - 300.0	8.560E 10	1.215E-02	1.833E-03	9.070E-04	4.684E-04	3.089E-04
300.0 - 350.0	5.400E 10	7.380E-03	1.382E-03	6.775E-04	3.246E-04	2.154E-04
350.0 - 400.0	3.039E 10	6.175E-03	1.001E-03	4.259E-04	2.807E-04	1.684E-04
400.0 - 450.0	2.298E 10	4.548E-03	7.290E-04	2.300E-04	2.317E-04	1.445E-04
450.0 - 500.0	1.821E 10	2.987E-03	6.375E-04	2.804E-04	2.308E-04	1.069E-04
500.0 - 600.0	9.410E 09	2.101E-03	4.370E-04	2.116E-04	1.433E-04	8.495E-05
600.0 - 800.0	4.248E 09	8.455E-04	2.275E-04	1.237E-04	6.740E-05	4.172E-05
800.0 - 1000.0	1.378E 09	3.428E-04	9.665E-05	4.964E-05	3.520E-05	2.433E-05
1000.0 - 1200.0	5.515E 08	1.540E-04	3.782E-05	2.387E-05	1.801E-05	1.000E-05
1200.0 - 1500.0	1.442E 08	4.732E-05	1.800E-05	8.835E-06	6.725E-06	3.398E-06
TOTAL ENERGY DEPOSITION/SEC	6.273E 19	8.844E 06	1.542E 06	7.707E 05	5.024E 05	3.063E 05

TABLE X. (Continued)

($keV\ m^{-3}\ sec^{-1}$/keV of source energy)

6.00 TO 7.00 MEV GAMMAS

RADIAL DISTANCE INTERVAL (METERS)	DELAY TIME (SEC) 1.50E-07 - 2.00E-07	2.00E-07 - 3.00E-07	3.00E-07 - 5.00E-07	5.00E-07 - 7.00E-07	7.00E-07 - 1.00E-06	1.00E-06 - 1.50E-06
.0 - 10.0	.000E 00	1.351E-03	1.500E-03	9.230E-04	4.093E-05	1.430E-03
10.0 - 20.0	3.618E-03	1.333E-03	5.860E-04	3.156E-04	3.263E-04	1.466E-04
20.0 - 40.0	2.155E-03	1.282E-03	6.400E-04	3.279E-04	1.810E-04	7.645E-05
40.0 - 60.0	1.037E-03	1.355E-03	6.710E-04	2.529E-04	2.118E-04	7.680E-05
60.0 - 80.0	8.760E-04	7.335E-04	4.418E-04	2.319E-04	1.315E-04	6.380E-05
80.0 - 100.0	1.165E-03	5.780E-04	3.295E-04	2.131E-04	1.063E-04	7.325E-05
100.0 - 125.0	8.800E-04	5.515E-04	2.591E-04	1.607E-04	9.855E-05	5.755E-05
125.0 - 150.0	7.485E-04	3.853E-04	2.108E-04	1.171E-04	8.745E-05	5.565E-05
150.0 - 175.0	5.045E-04	3.248E-04	2.258E-04	1.025E-04	6.830E-05	4.996E-05
175.0 - 200.0	3.544E-04	2.199E-04	1.613E-04	8.485E-05	7.030E-05	3.609E-05
200.0 - 250.0	2.990E-04	2.083E-04	1.022E-04	8.095E-05	5.505E-05	2.904E-05
250.0 - 300.0	1.730E-04	1.365E-04	8.020E-05	5.045E-05	3.504E-05	2.096E-05
300.0 - 350.0	1.639E-04	1.029E-04	5.810E-05	3.068E-05	2.514E-05	1.689E-05
350.0 - 400.0	1.056E-04	7.345E-05	4.805E-05	2.575E-05	2.082E-05	1.185E-05
400.0 - 450.0	9.905E-05	6.340E-05	3.553E-05	1.981E-05	1.347E-05	9.530E-06
450.0 - 500.0	5.555E-05	4.808E-05	2.779E-05	1.998E-05	1.075E-05	7.385E-06
500.0 - 600.0	5.160E-05	3.313E-05	1.868E-05	1.189E-05	7.200E-06	4.220E-06
600.0 - 800.0	2.827E-05	1.774E-05	1.011E-05	5.785E-06	3.775E-06	2.393E-06
800.0 - 1000.0	1.422E-05	8.970E-06	4.095E-06	2.634E-06	1.571E-06	1.014E-06
1000.0 - 1200.0	5.810E-06	4.751E-06	2.588E-06	1.088E-06	7.510E-07	4.647E-07
1200.0 - 1500.0	2.784E-06	1.799E-06	7.735E-07	4.776E-07	2.978E-07	1.714E-07
TOTAL ENERGY DEPOSITION/SEC	1.987E 05	1.333E 05	7.221E 04	4.219E 04	2.781E 04	1.716E 04

TABLE X. (Continued)

(keV $m^{-3} sec^{-1}$/keV of source energy)

6.00 TO 7.00 MEV GAMMAS
DELAY TIME (SEC)

RADIAL DISTANCE INTERVAL (METERS)	1.50E-06 - 2.00E-06	2.00E-06 - 3.00E-06	3.00E-06 - 5.00E-06	5.00E-06 - 7.00E-06	7.00E-06 - 1.00E-05
.0 - 10.0	.000E 00	.000E 00	.000E 00	.000E 00	.000E 00
10.0 - 20.0	3.587E-05	1.931E-05	1.087E-06	.000E 00	.000E 00
20.0 - 40.0	1.064E-04	2.123E-05	1.393E-06	4.439E-07	.000E 00
40.0 - 60.0	3.915E-05	1.572E-05	2.552E-06	7.440E-08	.000E 00
60.0 - 80.0	5.115E-05	1.667E-05	2.863E-06	1.452E-07	.000E 00
80.0 - 100.0	3.620E-05	1.585E-05	3.027E-06	3.400E-08	1.239E-09
100.0 - 125.0	3.596E-05	1.505E-05	2.767E-06	4.692E-08	.000E 00
125.0 - 150.0	2.796E-05	9.970E-06	2.177E-06	5.245E-08	2.794E-09
150.0 - 175.0	2.407E-05	1.104E-05	1.908E-06	6.955E-08	1.717E-10
175.0 - 200.0	2.250E-05	1.121E-05	1.374E-06	8.950E-08	1.120E-09
200.0 - 250.0	1.641E-05	7.610E-06	1.241E-06	6.150E-08	6.620E-10
250.0 - 300.0	1.338E-05	6.035E-06	1.049E-06	2.191E-08	3.145E-10
300.0 - 350.0	1.111E-05	4.481E-06	7.540E-07	3.938E-08	9.925E-10
350.0 - 400.0	8.275E-06	3.651E-06	5.940E-07	1.909E-08	2.368E-09
400.0 - 450.0	5.810E-06	2.656E-06	4.517E-07	3.173E-08	1.949E-09
450.0 - 500.0	4.626E-06	2.094E-06	3.172E-07	3.363E-08	2.192E-10
500.0 - 600.0	2.729E-06	1.393E-06	2.247E-07	1.240E-08	4.673E-10
600.0 - 800.0	1.376E-06	6.675E-07	1.215E-07	5.960E-09	1.262E-11
800.0 - 1000.0	6.630E-07	3.060E-07	5.420E-08	1.512E-09	1.304E-12
1000.0 - 1200.0	2.331E-07	1.156E-07	2.289E-08	8.280E-10	9.410E-13
1200.0 - 1500.0	9.860E-08	4.813E-08	8.825E-09	2.972E-10	.000E 00
TOTAL ENERGY DEPOSITION/SEC	1.039E 04	4.823E 03	8.332E 02	3.794E 01	7.965E-01

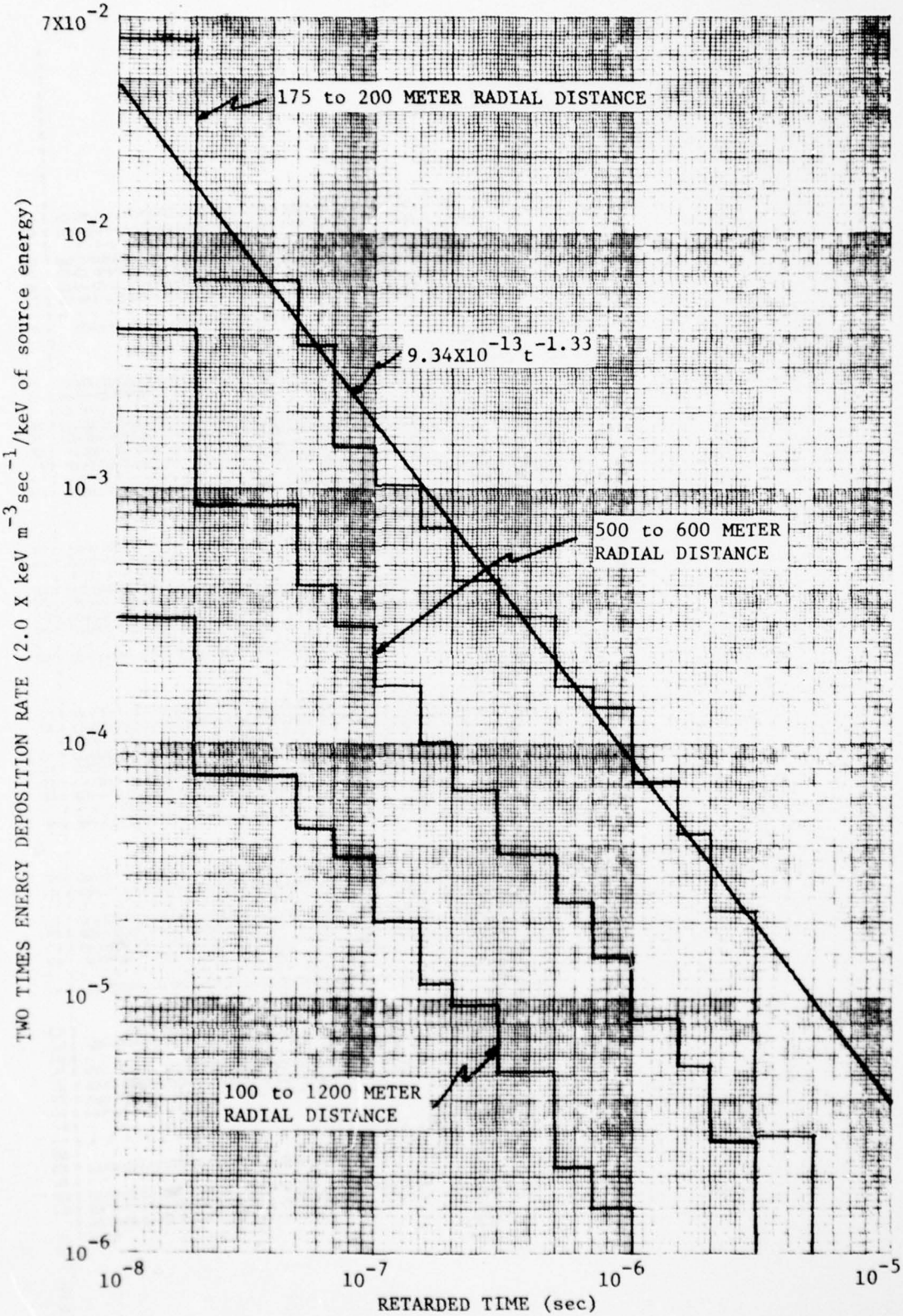

Fig. 8. Time Dependence of the Energy Deposition from a 6 to 7 MeV Point Isotropic Gamma-Ray Source

TABLE XI. TIME DEPENDENT NEUTRON ENERGY DEPOSITION RATE IN A 1500 METER RADIUS SPHERE AS A FUNCTION OF THE SOURCE ENERGY INTERVAL

(keV sec^{-1}/source neutron)

Time (sec)	UPPER BOUND OF SOURCE ENERGY INTERVAL (MeV)								
	.00335*	.0912	.0248	.0676	.184	.303	.500	.823	1.353
$0-2X10^{-7}$	7.127+3	3.715+4	1.104+5	3.645+5	1.122+6	4.018+6	6.998+6	1.288+7	2.194+7
$3X10^{-7}$	6.306+3	2.802+4	1.426+5	4.004+5	1.625+6	4.333+6	1.088+7	1.101+7	2.295+7
$5X10^{-7}$	7.439+3	2.226+4	5.848+5	4.030+5	1.936+6	3.800+6	8.617+6	9.498+6	1.982+7
$1X10^{-6}$	6.396+3	2.591+4	1.219+5	4.234+5	2.118+6	3.739+6	8.344+6	1.248+7	2.242+7
$2X10^{-6}$	7.091+3	3.544+4	1.361+5	4.687+5	1.623+6	3.321+6	8.382+6	1.053+7	2.215+7
$3X10^{-6}$	7.888+3	2.880+4	1.277+5	4.375+5	1.542+6	3.773+6	7.050+6	1.174+7	2.192+7
$5X10^{-6}$	8.434+3	3.432+4	1.187+5	4.306+5	1.549+6	3.058+6	7.254+6	1.022+7	2.069+7
$7X10^{-6}$	7.110+3	3.203+4	1.188+5	3.927+5	1.407+6	3.225+6	6.787+6	1.034+7	1.981+7
$1X10^{-5}$	6.840+3	2.685+4	1.055+5	4.107+5	1.417+6	3.010+6	6.459+6	9.543+6	1.740+7
$2X10^{-5}$	6.678+3	2.972+4	1.078+5	3.924+5	1.254+6	2.679+6	5.192+6	8.752+6	1.435+7
$3.5X10^{-5}$	6.448+3	2.565+4	9.329+4	3.327+5	1.023+6	2.240+6	3.855+6	7.179+6	1.156+7
5.0-5	5.574+3	2.427+4	7.996+4	2.696+5	8.463+5	1.809+6	2.923+6	5.461+6	8.595+6
7.0-5	5.140+3	2.087+4	7.039+4	2.281+5	6.642+5	1.334+6	2.044+6	3.888+6	6.346+6
1.0-4	4.978+3	1.800+4	5.593+4	1.703+5	4.958+5	9.272+5	1.422+6	2.366+6	4.057+6
2.0-4	3.738+3	1.273+4	3.655+4	9.484+4	2.422+5	4.263+5	5.957+5	8.970+5	1.418+6
4.04	2.229+3	6.313+3	1.463+4	3.086+4	6.209+4	9.375+4	1.261+5	1.655+5	2.188+5
7.0-4	1.102+3	2.393+3	4.458+3	7.553+3	1.192+4	1.524+4	1.832+4	2.112+4	2.543+4
1.0-3	5.331+2	9.896+2	1.521+3	2.195+3	2.946+3	3.633+4	3.904+3	4.219+3	4.595+3
2.0-3	1.880+2	2.955+2	3.978+2	5.097+2	6.235+2	7.117+2	7.372+2	7.620+2	7.839+2
3.5-3	4.212+1	5.638+1	6.442+1	7.614+1	8.441+1	8.914+1	9.089+1	9.091+1	9.035+1
keV/source neutron	2.134+0	6.239+0	1.680+1	4.602+1	1.257+2	2.425+2	4.007+2	6.610+2	1.089+3

*lower bound = 0.001 MeV

TABLE XI. (Continued)

(keV sec^{-1}/source neutron)

Time (sec)	UPPER BOUND OF SOURCE ENERGY INTERVAL (MeV)									
	1.738	2.232	2.865	3.680	6.070	7.790	10.0	12.0	13.5	15.0
$0-2X10^{-7}$	3.865+7	5.707+7	8.728+7	1.857+8	2.621+8	4.154+8	5.274+8	1.197+9	1.831+9	1.949+9
$3X10^{-7}$	4.438+7	5.465+7	8.677+7	1.697+8	2.782+8	4.021+8	4.741+8	1.292+9	1.527+9	1.470+9
$5X10^{-7}$	3.971+7	4.983+7	7.380+7	1.713+8	3.077+8	3.311+8	4.776+8	1.011+9	1.310+9	1.889+9
$1X10^{-6}$	4.229+7	5.187+7	7.338+7	1.799+8	2.688+8	3.988+8	5.403+8	9.258+8	1.312+9	1.494+9
$2X10^{-6}$	3.851+7	5.541+7	7.711+7	1.741+8	2.759+8	3.291+8	4.940+8	8.809+8	1.169+9	1.486+9
$3X10^{-6}$	3.471+7	4.951+7	7.787+7	1.559+8	2.631+8	3.160+8	4.283+8	6.834+8	1.004+9	1.092+9
$5X10^{-6}$	3.594+7	4.623+7	6.435+7	1.321+8	2.147+8	2.661+8	3.860+8	5.148+8	7.322+8	8.893+8
$7X10^{-6}$	3.275+7	4.489+7	6.661+7	1.136+8	1.891+8	2.394+8	3.026+8	4.391+8	4.942+8	5.596+8
$1X10^{-5}$	3.026+7	4.139+7	5.544+7	8.915+8	1.667+8	2.049+8	2.230+8	2.968+8	3.496+8	3.307+8
$2X10^{-5}$	2.320+7	3.472+7	4.424+7	6.023+8	1.073+8	1.342+8	1.410+8	1.418+8	1.420+8	1.482+8
$3.5X10^{-5}$	1.646+7	2.185+7	2.999+7	3.178+7	4.616+7	6.633+7	6.389+7	5.133+7	4.615+7	4.580+7
$5.0X10^{-5}$	1.119+7	1.418+7	1.852+7	1.778+7	1.949+7	2.624+7	2.730+7	2.064+7	1.717+7	1.743+7
$7.0X10^{-5}$	8.321+6	9.597+6	1.141+7	1.081+7	9.477+6	1.061+7	1.124+7	9.299+6	8.211+6	7.726+6
$1.0X10^{-4}$	5.095+6	5.872+6	6.459+6	5.846+6	4.507+6	4.388+6	4.370+6	4.025+6	3.795+6	3.430+6
$2.0X10^{-4}$	1.764+6	2.005+6	2.166+6	1.881+6	1.385+6	1.202+6	1.194+6	1.142+6	1.106+6	1.062+6
$4.0X10^{-4}$	2.496+5	2.704+5	2.669+5	2.254+5	1.533+5	1.340+5	1.398+5	1.330+5	1.270+5	1.281+5
$7.0X10^{-4}$	2.671+4	2.711+4	2.506+4	2.000+4	1.293+4	1.087+4	1.243+4	1.205+4	1.188+4	1.160+4
$1.0X10^{-3}$	4.648+3	4.574+3	3.892+3	3.069+3	1.929+3	1.727+3	2.007+3	1.936+3	1.846+3	1.877+3
$2.0X10^{-3}$	7.704+2	7.155+2	6.224+3	4.786+2	2.991+2	2.782+2	3.101+2	3.127+2	2.937+2	2.972+2
$3.5X10^{-3}$	8.366+1	8.008+1	6.777+1	5.168+1	3.109+1	3.089+1	3.278+1	3.452+1	3.178+1	3.264+1
keV/source neutron	1.545+3	1.985+3	2.532+3	3.245+3	4.679+3	5.885+3	6.773+3	8.346+3	9.895+3	1.095+4

TABLE XII. TIME DEPENDENT SECONDARY GAMMA-RAY ENERGY DEPOSITION RATE IN A 1500 METER RADIUS SPHERE OF AIR AS A FUNCTION OF THE NEUTRON SOURCE ENERGY INTERVAL

(keV $m^{-2}sec^{-1}$/source neutron)

TIME[a] (SEC)	UPPER BOUND OF NEUTRON SOURCE ENERGY INTERVAL (MeV)							
	0.00335*	0.0912	0.0248	0.0676	0.184	0.303	0.500	0.823	1.353
$2X10^{-7}$		0	0	0	0	0	0	0	2.707+4
$3X10^{-7}$		0	0	0	0	0	0	0	0
$5X10^{-7}$		0	0	0	0	0	0	0	0
$1.0X10^{-6}$		0	0	0	0	0	6.969+4	1.398+4	1.653+2
$2.0X10^{-6}$		0	0	0	0	0	1.519+3	2.940+4	1.064+2
$3.0X10^{-6}$		0	0	0	0	0	1.782+2	8.278+3	1.079+2
$5.0X10^{-6}$		0	0	0	0	0	1.694+2	1.120+4	9.229+3
$7.0X10^{-6}$		0	0	0	0	0	0	1.952+4	5.869+3
$1.0X10^{-5}$		0	0	0	0	0	4.723+4	1.515+4	6.867+3
$2.0X10^{-5}$		4.557+4	4.381+4	0	0	0	4.153+3	2.867+4	1.267+4
$3.5X10^{-5}$		0	0	0	0	2.438+3	2.434+3	1.649+4	1.592+4
$5.0X10^{-5}$		0	0	0	0	0	1.610+4	8.949+3	1.696+4
$7.0X10^{-5}$		0	6.529+4	9.603+1	2.013+4	0	1.994+4	8.720+3	1.160+4
$1.0X10^{-4}$		0	4.402+4	0	1.038+4	0	9.184+1	2.343+3	1.311+4
$2.0X10^{-4}$		8.907+3	0	0	1.276+4	2.424+3	6.224+3	5.916+3	1.288+4
$4.0X10^{-4}$		4.538+3	6.654+3	6.566+3	1.099+4	1.291+4	1.994+3	8.023+3	9.335+3
$7.0X10^{-4}$		3.068+3	1.494+3	1.273+4	1.336+4	7.348+3	1.169+4	4.263+3	4.004+3
$1.0X10^{-3}$		4.477+3	4.631+3	7.332+3	5.895+3	5.959+3	8.998+4	7.155+3	5.371+3
$2.0X10^{-3}$		8.152+3	5.965+3	5.415+3	7.158+3	8.013+3	7.181+3	4.139+3	6.116+3
$3.5X10^{-3}$		7.568+3	5.112+3	5.999+3	5.270+3	6.467+3	6.902+3	5.597+3	4.174+3
$1.5X10^{-2}$		6.123+3	6.087+3	6.549+3	6.623+3	6.442+3	5.744+3	5.345+3	6.053+3
$1.0X10^{-1}$		3.131+3	3.053+3	3.024+3	2.991+3	2.820+3	2.859+3	2.918+3	2.643+3
keV/source neutron		3.606+2	3.494+2	3.545+2	3.554+2	3.383+2	3.347+2	3.287+2	3.144+2

*lower bound of interval = 0.001 MeV

a. Lower Bound of Time Interval

TABLE XII. (Continued)

(keV sec^{-1}/source neutron)

TIME (SEC)	UPPER BOUND OF NEUTRON SOURCE ENERGY INTERVAL (MeV)									
	1.738	2.232	2.865	3.680	6.070	7.790	10.00	12.00	13.5	15.0
$2X10^{-7}$	2.798+4	2.572+4	1.557+5	1.122+6	1.813+7	1.063+8	2.287+8	3.563+8	5.853+8	3.715+8
$3X10^{-7}$	2.445+2	1.158+4	1.657+5	6.018+5	3.600+7	9.793+7	8.931+7	4.896+8	3.601+8	6.360+8
$5X10^{-7}$	2.804+4	2.966+4	2.039+5	6.924+5	2.532+7	1.103+8	2.234+8	4.199+8	4.526+8	4.085+8
$1X10^{-6}$	3.372+4	3.679+4	1.410+5	9.270+5	2.092+7	1.453+8	2.011+8	4.201+8	3.712+8	3.801+8
$2X10^{-6}$	1.713+4	1.587+4	1.157+5	1.096+6	2.308+7	1.255+8	2.211+8	3.728+8	3.633+8	4.326+8
$3X10^{-6}$	3.345+4	2.456+4	1.229+5	8.290+5	2.452+7	1.554+8	2.001+8	3.405+8	3.755+8	3.880+8
$5X10^{-6}$	1.663+4	4.000+4	7.545+4	6.565+5	1.603+7	8.063+7	1.980+8	2.387+8	2.780+8	2.481+8
$7X10^{-6}$	2.781+4	2.509+4	6.778+4	6.036+5	1.536+7	7.636+7	1.867+8	2.353+8	2.147+8	1.720+8
$1X10^{-5}$	9.404+3	3.511+4	7.466+4	5.263+5	1.206+7	5.775+7	1.225+8	1.330+8	1.474+8	1.308+8
$2X10^{-5}$	1.558+4	2.190+4	4.933+4	1.979+5	5.278+6	2.695+7	5.652+7	7.156+7	5.372+7	4.895+7
$3.5X10^{-5}$	1.631+4	1.280+4	2.270+4	4.631+4	1.687+6	6.690+6	1.205+7	1.174+7	8.412+6	8.663+6
$5.0X10^{-5}$	1.425+4	1.747+4	1.642+4	1.675+4	2.692+5	8.041+5	2.305+6	1.547+6	9.940+5	7.443+5
$7.0X10^{-5}$	1.932+4	1.016+4	1.078+4	9.919+3	2.348+4	1.472+5	3.423+5	1.820+5	1.240+5	8.577+4
$1.0X10^{-4}$	6.755+3	1.196+4	1.414+4	8.668+3	5.843+3	1.042+4	1.653+4	1.911+4	6.895+3	6.050+3
$2.0X10^{-4}$	3.092+3	4.152+3	3.875+3	4.745+3	2.552+3	1.889+3	1.174+3	1.794+3	1.292+3	2.051+3
$4.0X10^{-4}$	7.739+3	3.924+3	4.199+3	5.620+3	4.036+3	2.089+3	3.112+3	1.953+3	1.784+3	1.326+3
$7.0X10^{-4}$	4.690+3	2.972+3	0	2.831+3	1.052+3	1.905+3	2.565+3	3.815+3	3.268+3	1.781+3
$1.0X10^{-3}$	4.807+3	2.990+3	3.880+3	2.037+3	2.284+3	2.965+3	3.293+3	1.567+3	9.251+2	6.121+3
$2.0X10^{-3}$	5.676+3	4.461+3	3.492+3	3.371+3	2.715+3	2.031+3	2.011+3	2.521+3	1.458+3	1.999+3
$3.5X10^{-3}$	7.151+3	5.858+3	4.095+3	2.893+3	1.601+3	2.443+3	1.794+3	2.441+3	1.844+3	2.314+3
$1.5X10^{-2}$	5.559+3	4.622+3	4.199+3	3.036+3	1.609+3	1.515+3	1.711+3	2.050+3	1.664+3	2.208+3
$1.0X10^{-1}$	2.290+3	2.189+3	1.763+3	1.508+3	8.495+2	8.773+2	9.420+2	9.666+2	8.476+2	9.709+2
keV/source neutron	2.811+2	2.570+2	2.128+2	1.842+2	3.500+2	1.379+3	2.653+3	3.508+3	3.374+3	3.212+3

last time interval ($1.5X10^{-2}$ to $1.0X10^{-1}$ sec) when the neutron source energy is less than 3.68 MeV, When the source energy is above 3.68 MeV, most of the secondary gamma-ray energy deposition comes from inelastic gammas and is produced by neutrons that have undergone inelastic collisions before about $5X10^{-5}$ seconds. The total secondary gamma-ray energy deposited within the 1500 m radius decreases slowly with an increase in the neutron source energy until the neutron source energy exceeds 3.68 MeV after which it increases to a maximum for neutrons in the 12.0 to 13.5 MeV interval and then reduces with increasing energy.

Of interest to a number of organizations working on problems relating to exposure of personnel and equipment to the radiations produced by nuclear sources is the time-dependent energy deposition vs range in air for point isotropic sources and the time-independent energy deposition vs range for line-beam sources. The time-dependent energy depositions in the 21 radial intervals between 0 and 1500 meters listed in Table II for point isotropic nuclear sources emitting in the discrete-energy intervals listed in Table IV are tabulated in Vols. II, III, and IV for primary gammas, neutrons and neutron-induced secondary gamma rays respectively. The energy deposition data given in Vols. II through IV have the following units:

Vol. No.	Source	Units of Energy Deposition Data
II	gamma rays	keV m^{-3} sec^{-1}/keV of source energy
III	neutrons	keV m^{-3} sec^{-1}/source neutron
IV	secondary gamma rays	keV m^{-3} sec^{-1}/source neutron

The radial distances are in meters and the retarded times are in seconds. For the gamma-ray sources, the energy deposition in the 0-to-10^{-20}-second delay-time interval is taken to be produced by the first-order scattering and absorption interactions undergone by the direct radiation. The gamma-ray energy deposition computed for retarded times greater than 10^{-20} seconds in a given radial interval is that produced by gamma rays that underwent their first-order collision outside of the deposition volume and then underwent second-order or greater collision within the deposition volume.

The time-integrated total energy deposition data vs radial distance and source-energy interval are also listed in Vols. II, III and IV for point-isotropic gamma-ray, neutron and neutron-produced secondary gamma-ray sources, respectively. The units for the gamma-ray energy deposition data are keV m^{-3}/keV of source energy. The units for the neutron and secondary gamma-ray energy deposition data are keV m^{-3}/source neutron.

The time-integrated energy deposition data for line-beam sources as a function of radial distance, deposition polar-angle interval (Table II) and source-energy interval have been curve fitted by a least squares method with the use of the equation

$$ED(\theta_i, \bar{R}_j, E_k) = e^{-A_{i,k}} \bar{R}_j^{B_{i,k}} e^{-C_{i,k} \bar{R}_j}$$

where i and k are indices denoting the deposition polar angle interval and source energy interval and

$$\bar{R}_j = \left[\frac{1}{2} (R_{j-1}^3 + R_j^3) \right]^{1/3}$$

for R_{j-1} and R_j being the lower and upper bounds of the jth radial interval. The parameters A, B and C and the coefficient of determination r^2 as a function of the deposition polar angle and source energy intervals are given in Vol. V. Values of r^2 close to 1.00 indicate the goodness of the fit to the DEPO-calculated energy deposition data. The energy deposition, $ED(\theta_i, \bar{R}_j, E_k)$ is in units of keV m^{-3}/keV of source energy for gamma-ray sources and keV m^{-3}/source neutron for neutron and secondary gamma-ray sources.

The time-integrated energy deposition data given in Vols. II through V can be converted to air kerma rate (exposure rate in air, $\rho = 1.225 \times 10^{-3}$ g/cm^3) by multiplying the energy deposition data with one of the following factors:

Source	Kerma Factor
Gamma Rays	$4.708X10^{-11}\ \bar{E}_o$
Neutrons	$4.708X10^{-11}$
Secondary Gamma Rays	$4.708X10^{-11}$

The units of the resulting air-kerma rate is rad hr^{-1}/source particle sec^{-1} and $\bar{E}_o$ is the average source energy within the source energy interval.

III. ENERGY DEPOSITION DATA FOR CONICAL SOURCES

A modified version of the DEPO program was developed for use in determining the spatial and time distributions of the nuclear energy deposited in an infinite air medium for conical sources from the data generated for line-beam sources. For each point of energy deposition recorded on a ZAP, ZAPN or ZAPGAM history tape for each of the monodirectional sources, a cosine value between the limits of the conical source bounds was selected at random (see ψ_i in Fig. 1). The new direction selected is considered to be the new source direction and the polar displacement angle, θ_E, from the monodirectional source was referenced to this new source direction. A number of random azimuthal angles, γ, about the new source direction was selected uniformly between 0 and 2π. The number of azimuthal angles selected was established as

$$N = 2 \cdot IFIX(\frac{\alpha}{\pi} \arccos\theta_E) + 3$$

where α was slightly less than 5. The number of points of energy deposition (each depositing $\frac{1}{N}$ of the original energy deposition) ranged between 3 and 11. The third side of the spherical triangle, β, references the points of energy deposition back to the axis of the conical source. The angular position of the energy deposition for a conical source was recorded in terms of the angle β, the angle between the point of deposition and the axis of the conical source. The radial distance and the time to collision was taken to be the same as that computed for the monodirectional source.

The bounds of the source polar angle intervals for the conical sources are 0-5, 5-10, 10-20, 20-30, 30-40, 40-50, 50-60, 60-70, 70-80, and 80-90 degrees. Deposition data were generated with the revised version of DEPO for conical source polar angles up to 90^o. Energy deposition data for conical source polar angles ψ_i greater than 90^o can be obtained by reordering the polar angle intervals in the deposition geometry. The new deposition polar angle bounds θ'_k for k = 0, 21 are defined by $\theta'_k = 180^o - \theta_{21-k}$ when $90 < \theta_s \leq 180^o$.

Energy deposition data for source polar-angle bounds, ψ_d, for a conical source between 100^o and 110^o are the same data as those computed for conical source polar-angle bounds of 70^o and 80^o with the deposition polar angles θ'_k for the 100^o to 110^o conical source defined as given above in terms of the deposition polar angles θ_{21-k} for the 70^o to 80^o conical sources.

IV. RENDER PROCEDURE

A computer procedure, designated as RENDER, was developed for use in computing the time and spatial dependent nuclear energy deposition in the atmosphere for time, energy and direction dependent point sources.

The energy deposition at spatial position $\theta_i \leq \theta \leq \theta_{i+1}$ and $r_j \leq r \leq r_{j+1}$ and time τ is given by the integral equation

$$R(\theta_i \leq \theta_{i+1},\ r_j \leq r \leq r_{j+1},\ \tau) =$$

$$\frac{\int_E \int_{\phi=0}^{2\pi} \int_{\theta_i}^{\theta_{i+1}} \int_{r_j}^{r_{j+1}} \int_{\psi=0}^{\pi} \int_0^{\tau} S(E,\psi,t)\ T(E,\theta,r,\psi,\tau-t)\sin\psi r^2 \sin\theta dt d\psi dr d\theta d\phi dE}{\int_{\phi=0}^{2\pi} \int_{\theta_i}^{\theta_{i+1}} \int_{r_j}^{r_{j+1}} \int_{\psi=0}^{\pi} \sin\psi r^2 \sin\theta d\psi dr d\theta d\phi} \qquad (1)$$

where $S(E,\psi,t)$ is the energy, direction and time-dependent source term

$T(E,\theta,r,\psi,\tau-t)$ is the energy deposited per unit volume for initial source energy E emitted in direction ψ and deposition occurring at position r,θ and time $\tau-t$.

The convolution integral portion of Equation (1)

$$\int_0^{\tau} S(E,\psi,t)\ T(E,\theta,r,\psi,\tau-t)dt \qquad (2)$$

is evaluated in RENDER by assuming analytical functions for the source $S(E,\psi,t)$ and the transmission $T(\tau-t)$. Ignoring the dependence on source conical angle ψ, source energy E and spatial location r,θ we can rewrite

the above equation as

$$R(\tau) = \int_0^{\tau} S(t)\ T(\tau-t)dt \quad , \tag{3}$$

where $S(t)$ and $T(\tau-t)$ are analytic functions. In practice, however, source values are given at discrete time points, say μ_i; transmission data is available as average arrival rates between two retarded times, say x_{j-1} and x_j. Considering these partical constraints and the fact that the convolution resultant R is to be defined at retarded times τ, a transformation of variables was made in Eq. 3 as

$$x = \tau - t \quad ,$$

thus

$$R(\tau) = \int_0^{\tau} T(x)\ S(\tau-x)dx \quad . \tag{4}$$

Since $T(x)$ is given as a constant (average) between time limits, say $\overline{T}\ (x_j)$, Eq. 4 can be written as

$$R(\tau) = \overline{T}(x_1) \int_0^{x_1} S(\tau-x)dx + \cdots + \overline{T}(x_j) \int_{x_{j-1}}^{\tau} S(\tau-x)dx$$

$$= \sum_{j=1}^{J} \overline{T}(x_j) \int_{x_{j-1}}^{\min(\tau,x_j)} S(\tau-x)dx \tag{5}$$

where $x_o \equiv 0$ and J is the index of the inequality

$$x_{J-1} < \tau \leq x_J \quad .$$

Reversing the previous change of variables gives

$$u = \tau - x$$

thus

$$R(\tau) = \sum_{j=1}^{J} \bar{T}(x_j) \int_{\tau-\min(\tau,x_j)}^{\tau-x_{j-1}} S(u)du \quad . \tag{6}$$

The integral part of Eq. 6 could be solved in a number of ways. Although the form of S was assumed to be

$$S(u) = aue^{-bu} \quad , \tag{7}$$

the RENDER program was written such that only minor programming changes would be necessary if another form of S were considered to be more applicable. Coefficients a and b in Eq. 5 are regenerated for each pair of source times, u_i and u_{i+1}, as

$$b = \frac{1}{u_{i+1}-u_i} \ln\left(\frac{S_i}{S_{i+1}} \cdot \frac{u_{i+1}}{u_i}\right)$$

and

$$a = \frac{S_i}{u_i} e^{b u_i} \quad .$$

These coefficients cause S(u) to be

$$S_i = a u_i e^{-b u_i}$$

and

$$S_{i+1} = a u_{i+1} e^{-b u_{i+1}} \quad .$$

Results of the integral portion of Eq. 6 follow as

$$\int S(u)du = \frac{a}{b^2} e^{-bu} (bu+1) \quad .$$

Convolution results can thus be obtained as

$$R(\tau) = \sum_{j=1}^{J} \overline{T}\,(x_i) \sum_{i=I_1}^{I_2} \frac{a}{b^2} \left[e^{-bU'_{1,i}} (bU'_{1,i}+1) - e^{-bU_{2,i}} (bU_{2,i}+1) \right] \quad (8)$$

where I_1 and I_2 are developed from the following inequalities

$$u_{I_1} < \tau - \min(\tau, x_j) \leq u_{I_1+1}$$

$$u_{I_2} < \tau - x_{j-1} \leq u_{I_2+1}$$

and

$$u_o \equiv 0 \quad .$$

Values of $U'_{1,i}$ and $U_{2,i}$ are give by

$$U'_{1,i} = \max(\tau - \min(\tau, x_j),\ u_{I_2+1-i})$$

$$U_{2,i} = \min(\tau - x_{j-1},\ u_{I_2+2-i})$$

and coefficients a and b are generated at each new value of i, with the exception of i = 0. The form of the source term in Eq. 7, considered on the interval $0 \leq u < \infty$, has some important properties. First

$$\frac{d}{du} S(u) = 0 \quad \text{when } u = \frac{1}{b}$$

$$\frac{d^2}{du^2} S\left(u = \frac{1}{b}\right) = -\frac{ab}{c}$$

which for a>0, b>0 gives a single maximum at $u=\frac{1}{b}$.

Secondly

$$\lim_{u\to\infty} S(u) = \lim_{u\to\infty} \frac{au}{e^{bu}} = \lim_{u\to\infty} \frac{\frac{d}{du}(au)}{\frac{d}{du}(e^{bu})} = \frac{0}{\infty} = 0$$

and

$$S(u=0) = a\cdot 0\cdot e^{-b(0)} = 0 \quad .$$

Thus the form of the source has the correct boundary conditions and contains one maximum.

To test the effectiveness of the numerical solution of the convolution process, an analytic source and transmission were chosen as

$$S(u) = 10^{12}\ u\ e^{-10^6 u}$$

$$T(x) = 2X10^5\ e^{-2X10^5 x}$$

which gives

$$R(\tau) = 3.125X10^5\ e^{-2X10^5\tau}\ \{1 - e^{-8X10^5\tau}\ [8X10^5\tau+1]\} \quad .$$

Graphs of S, T and R are shown in Fig. 9. Since the form of the source was identical to the assumed form of the source, it would seem reasonable that the results of the numerical solution be independent of the range of the source or the number of discrete values used (minimum of two are necessary to evaluate the coefficients a and b). This was indeed the case. The only errors possible were in 1) computer accuracy and 2) limiting values used to generate the average transmission value from

$$\overline{T}(x_j) = \frac{\int_{x_{j-1}}^{x_j} T(x)dx}{\int_{x_{j-1}}^{x_j} dx} = \frac{e^{-2X10^5 x_{j-1}} - e^{-2X10^5 x_j}}{x_j - x_{j-1}}$$

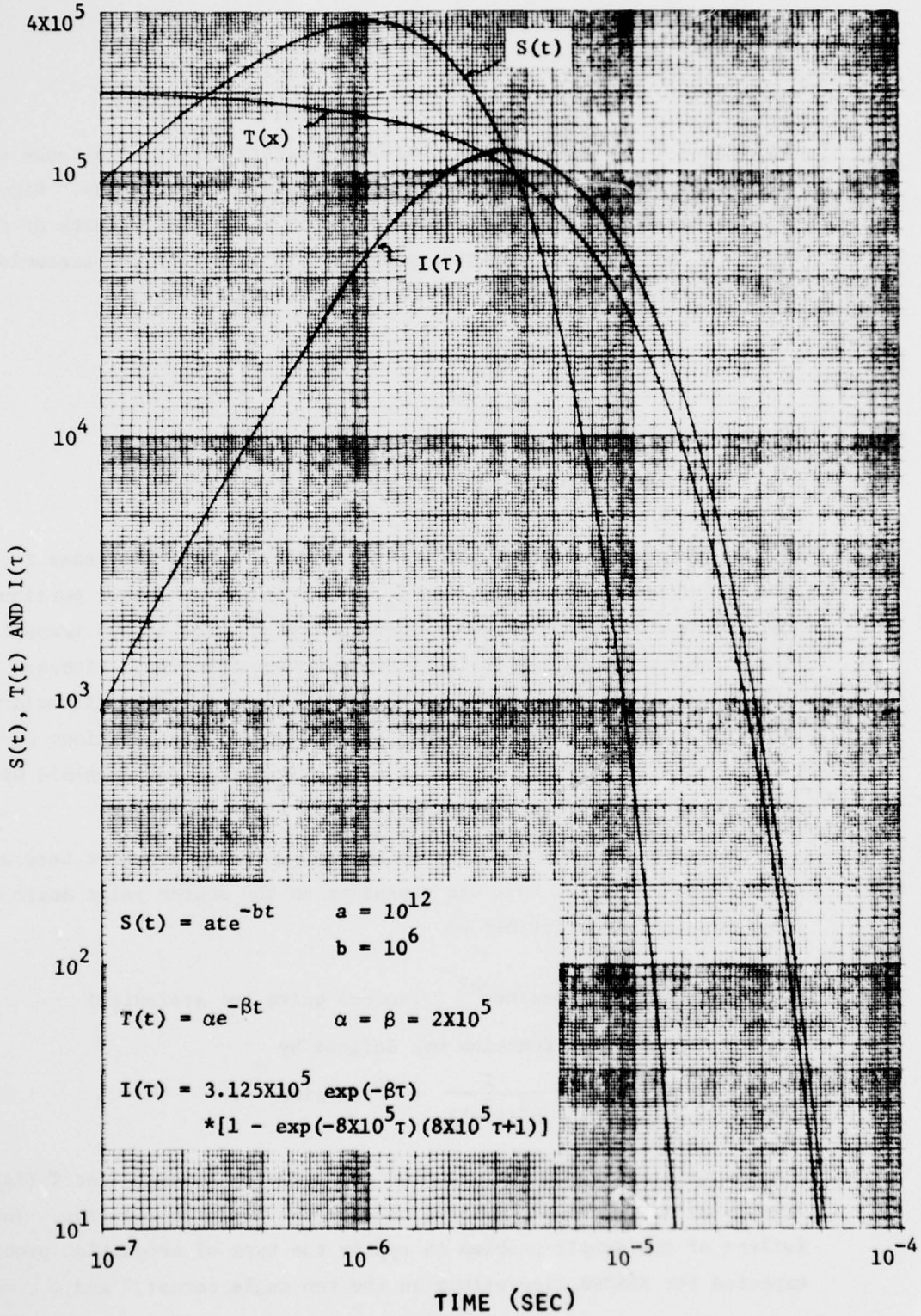

Fig. 9. Analytic Functions used in Test Problem

where $x_o \equiv 0$. Assuming small computer accuracy errors, the range of $\{x_i\}$ was varied but the number of x_i was held constant at 30. Figure 10 gives a tabulation of the per cent error in the RENDER results of five numerical solutions of the test problem. In each case the transmission time bounds were calculated as

$$x_j = X_o e^{j*\Delta}$$

where Δ was defined as

$$5*10^{-5} = X_o e^{30*\Delta} \quad .$$

X_o was input as 10^{-5}, 10^{-6}, 10^{-7}, 10^{-8} and 10^{-9}. This increase in the range of x_i gave two effects; as X_o became smaller a larger portion of the transmission function was defined but each value of the transmission became less accurate due to the increased time coverage. Although the transmission time set $\{x_i\}$ will, in practice, be fixed, it is evident that the X_o should be small enough to include all contributions to the transmission at early times and as many values of x_i as possible within computer memory storage requirements.

A second sample RENDER problem was run using a source term and transmission function that was dependent on the source polar angle ψ. The source term was defined by

$$S(\psi,t) = (1+\cos\psi)te^{-at} \quad \text{(source units per steradian)}$$

and the transmission function was defined by

$$T(\theta,\psi,r,t,E) = \frac{1}{r^2(r^2+1)} \; e^{-\gamma t}\sin\theta\sin\psi \quad . \tag{9}$$

A value of $\gamma = 455.8866187$ was used and symmetry in angle for T (ie. $T(\pi-\theta,\pi-\psi) = T(\theta,\psi)$ was employed to ease the analytic solution. The failure of the sample problem to typify the type of production problems expected for RENDER lies mainly in the two angle terms: θ and ψ . A

RETARDED TIME	Percent Error: Lower Bound of X_o (sec)				
τ(sec)	10^{-5}	10^{-6}	10^{-7}	10^{-8}	10^{-9}
1.1000E-07	-58.04	-9.91	-.48	-.01	-.01
1.2000E-07	-58.02	-9.84	-.41	-.01	-.02
1.4000E-07	-57.96	-9.72	-.30	-.01	-.02
1.6000E-07	-57.90	-9.59	-.22	-.02	-.02
1.8000E-07	-57.84	-9.47	-.18	-.02	-.03
2.1000E-07	-57.75	-9.27	-.13	-.02	-.03
2.3000E-07	-57.69	-9.14	-.11	-.02	-.03
2.7000E-07	-57.57	-8.88	-.08	-.03	-.04
3.0000E-07	-57.48	-8.68	-.06	-.03	-.05
3.4000E-07	-57.35	-8.42	-.05	-.03	-.04
3.9000E-07	-57.19	-8.08	-.05	-.04	-.06
4.4000E-07	-57.03	-7.73	-.04	-.04	-.07
5.0000E-07	-56.83	-7.31	-.04	-.05	-.07
5.6000E-07	-56.63	-6.87	-.04	-.05	-.09
6.4000E-07	-56.36	-6.28	-.04	-.07	-.10
7.4000E-07	-56.00	-5.51	-.04	-.06	-.10
8.2000E-07	-55.71	-4.88	-.04	-.08	-.14
9.4000E-07	-55.25	-3.90	-.05	-.09	-.14
1.0000E-06	-55.01	-3.40	-.05	-.08	-.13
1.2000E-06	-54.19	-1.69	-.06	-.13	-.22
1.3000E-06	-53.76	-1.08	-.06	-.11	-.22
1.5000E-06	-52.85	-.32	-.07	-.17	-.21
1.7000E-06	-51.87	.09	-.10	-.14	-.33
1.9000E-06	-50.83	.29	-.09	-.20	-.32
2.2000E-06	-49.14	.43	-.13	-.21	-.33
2.5000E-06	-47.28	.45	-.15	-.27	-.53
2.8000E-06	-45.23	.42	-.13	-.34	-.38
3.2000E-06	-42.20	.35	-.22	-.29	-.53
3.6000E-06	-38.80	.27	-.17	-.50	-.85
4.2000E-06	-32.92	.18	-.18	-.31	-.30
4.8000E-06	-26.02	.10	-.36	-.72	-1.10
5.4000E-06	-17.98	.01	-.17	-.16	-1.20
6.0000E-06	-8.69	-.07	-.48	-.89	.11
6.8000E-06	5.90	-.14	-.26	-.32	-1.66
7.8000E-06	28.19	-.19	.01	-1.00	-1.39
8.8000E-06	55.78	-.24	-.77	-.75	1.31
1.0000E-05	97.43	-.27	.44	-.19	-3.55
1.1000E-05	127.72	-.00	-1.08	-2.35	-1.87
1.2000E-05	101.19	.32	1.51	1.97	6.64
1.4000E-05	38.16	.61	-.32	-3.14	-5.45
1.6000E-05	11.25	.89	-1.32	7.13	2.92
1.8000E-05	3.07	1.75	6.06	-2.51	13.37
2.0000E-05	.83	1.45	-2.73	.01	-10.01
2.3000E-05	.22	3.66	5.77	5.55	16.87
2.6000E-05	.10	3.99	4.35	-1.50	20.86
3.0000E-05	.36	8.45	-5.65	19.22	-8.35
3.4000E-05	.21	11.63	26.96	-1.88	85.76
3.8000E-05	.56	7.01	-.65	92.22	4.87
4.4000E-05	.21	22.55	-7.06	-8.03	26.47
5.0000E-05	2.84	29.67	88.67	180.84	315.42

Fig. 10. Percent Error in RENDER Calculation for Sample Problem As a Function of the Lower Bound of X_o

transmission term which is separable in θ and ψ is obviously not representative of nature and a simple sine dependence does not reflect the variations found in the transmission data which has been previously generated. A more suitable dependence on the source and deposition angle would possibly have been a function of the form

$$T(\theta,\psi) = \exp\left[k\left|\sin^{n}(\psi-\theta)\right|\right] \quad .$$

Use of such a function would, however, complicate the analytic solution to such a degree that numerical methods would be required to obtain results. This would negate the purpose of the sample problem. Employment of the simple function (Eq. 9) will produce errors, but predictable errors which can be used to both demonstrate inherent errors of the procedure as well as the accuracy of the procedure to generate the appropriate solution. The desired solution is

$$R(\theta_i \le 0 \le \theta_{i+1},\ r_j \le r \le r_{j+1},\ \tau,\ E_K \le E \le E_{K+1}) =$$

$$\frac{3\pi}{4} \frac{(\theta_{i+1}-\theta_i + \cos\theta_i \sin\theta_i - \cos\theta_{i+1}\sin\theta_{i+1})(\tan^{-1} r_{j+1} - \tan^{-1} r_j)}{(\cos\theta_i - \cos\theta_{i+1})(r_{j+1}^3 - r_j^3)} \times$$

$$\frac{\{e^{-a\tau}[(\gamma-a)\tau+1] + e^{-\gamma\tau}\}}{(\gamma-a)^2} \quad .$$

To allow the source and transmission to be input to RENDER, bounds were established for all variables. There were 34 equally spaced source angle intervals ψ such that $0 \le \psi \le \pi$ and 20 source times t equally spaced in logarithm such that $10^{-8} \le t \le 10^{-5}$ seconds. Transmission data was defined for 17 source angles ψ such that $0 \le \psi \le \frac{\pi}{2}$, 50 times t such that $10^{-8} \le t < 10^{-2}$, radial and deposition angles as shown in Table XIII. Both source and transmission were independent of energy.

TABLE XIII. SAMPLE PROBLEM PARAMETERS

Interval Number	Output Polar Angle Interval (degrees)	Radial Interval (meters)	Deposition Polar Angle Interval (degrees)
1	0 - 1	0 - 10	0 - 1
2	1 - 2	10 - 20	1 - 2
3	2 - 5	20 - 40	2 - 3
4	5 - 10	40 - 60	3 - 5
5	10 - 20	60 - 80	5 - 7
6	20 - 30	80 - 100	7 - 10
7	30 - 40	100 - 125	10 - 15
8	40 - 60	125 - 150	15 - 20
9	60 - 70	150 - 175	20 - 30
10	70 - 80	175 - 200	30 - 40
11	80 - 90		40 - 50
12	90 - 100		50 - 60
13	100 - 110		60 - 70
14	110 - 120		70 - 80
15	120 - 130		80 - 90
16	130 - 150		90 - 100
17	150 - 160		100 - 120
18	160 - 170		120 - 140
19	170 - 175		140 - 160
20	175 - 180		160 - 180

Since the results of the analytic solution were separable in all variables, errors were also separable.
Consider first the time dependent error,

$$\xi(\tau) = \left\{ \frac{\sum_j \left[\frac{\int_{x_j}^{x_{j+1}} T(x)dx}{\int_{x_j}^{x_{j+1}} dx} \right] \int_{\tau-x_{j+1}}^{\tau-x_j} S(t)dt}{\int_0^{\tau} S(t)T(\tau-t)dt} - 1 \right\} * 100. \qquad (10)$$

Comparing results from RENDER and the analytic solution for this sample problem, these errors were found to be negligible before times around .1 msec but they steadily increase with time and by 10 msec have reached 82.86 per cent. This error is shown in Fig. 11 which is the time dependent results for radial interval between 125 to 150 meters and deposition angle interval between 80 to 90 degrees. The upper curve in the figure shows data from RENDER, the lower curve shows analytic solution results. To verify that the error was indeed a result of the phenomenon described by Equation 10, numerical evaluation was made with the same time bounds $\{x_j\}$ that were used for input to RENDER and a value $\tau = .01$ second. Evaluation of the integral over the source term only in Eq. 10 was made at the end points since the source was analytically integrable;

$$\int_{\tau-x_{j+1}}^{\tau-x_j} S(t)dt = \frac{1}{a^2} \left[(au_1+1)\, e^{-au_1} - (au_2+1)\, e^{-au_2} \right] \qquad (11)$$

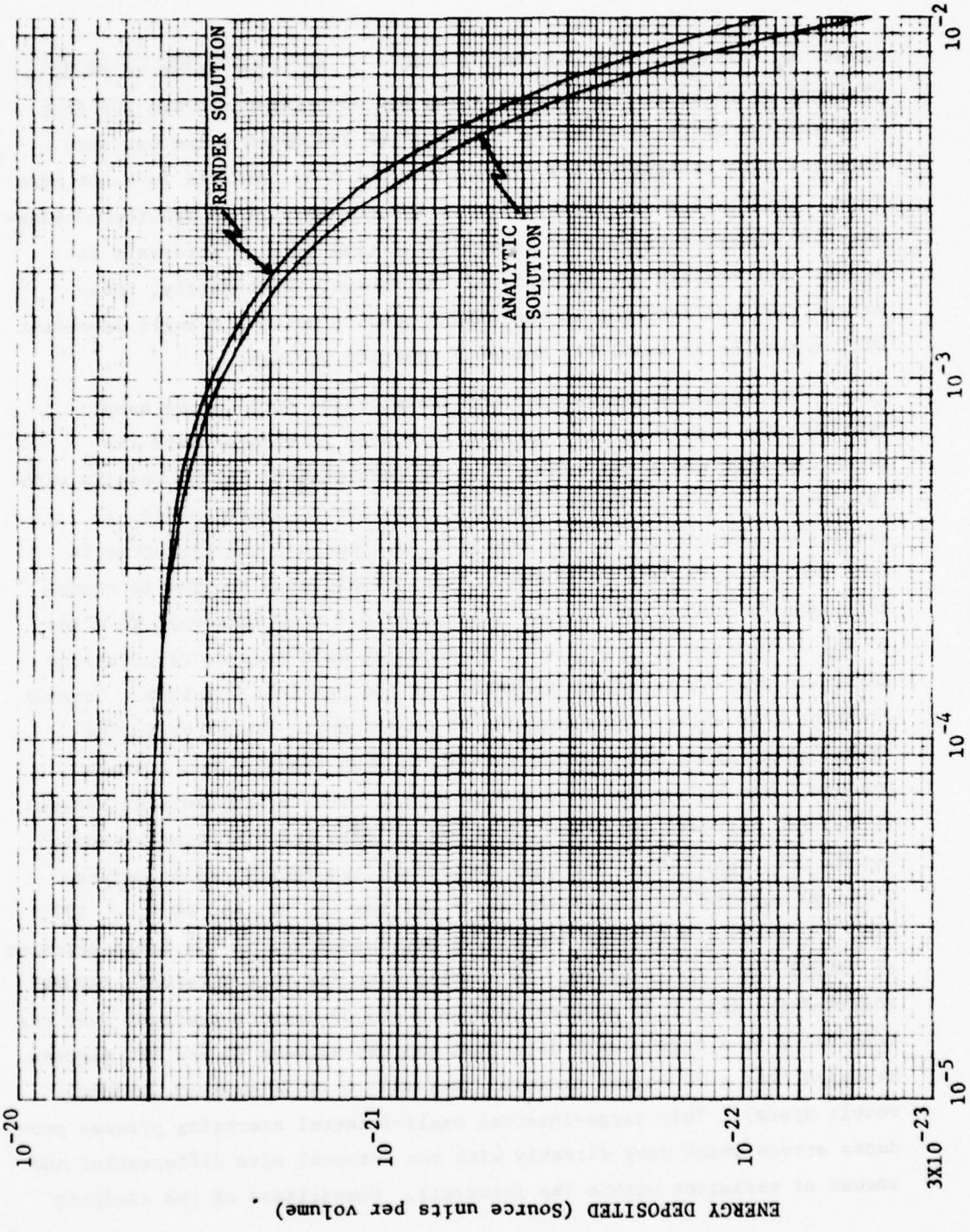

Fig. 11. Time Dependent Sample Problem Results for $125 \leq R \leq 150$ Meters, $80 \leq \theta \leq 90$ degrees

where $u_1 = \tau - x_{j+1}$, $u_2 = \tau - x_j$ and $a = 10^6$. An error value of 84.20 per cent resulted from this evaluation but more important was the fact that for the first 49 elements of $\tau - x_j$, the evaluated value was zero. Only the 50th element of $\tau - x_j$ (ie. .01 - .01 = 0) resulted in a non zero term. This type error is inherent to RENDER and will be manifested whenever the larger intervals of transmission time develop intervals in Eq. 11 that contain the majority of the source. Fortunately, those errors that are inherent in the RENDER results which are angle dependent will typically be small for normal production problems.

The angle dependencies of the transmission data in the sample problem were such that very large errors were introduced into the output of RENDER. A comparison of some intermediate RENDER results with the limiting function of the analytic solution is shown in Fig. 12 where the smooth curve is the analytic solution and the histogram is from intermediate data in RENDER. This normalized histogram is representative of RENDER results for all radial and time intervals when the source is between $0^\circ \leq \psi \leq 90^\circ$. As shown in this figure, results from RENDER accurately represent the shape of the analytic solution. Careful checking also showed the magnitude to be correct. The error in the RENDER calculation was finally introduced when results from sources between 0 and 90 degrees were combined with results from sources between 90 and 180 degrees. For the latter set of data the transmission angle set is reversed. Thus, for data resulting from source angles between 0 and 90 degrees the deposition angle set was {0, 20, 40, 60, ..., 177, 178, 179, 180}. The first deposition angle interval in the final printout of RENDER was 0 to 1 degree. To develop data for that interval, RENDER combined the data from sources between 0 and 90 degrees averaged over the interval 0 to 1 degree with data from sources between 90 and 180 degrees averaged over a 20 degree interval (actually 0 to 20 degrees in final-result space). This large-interval small-interval averaging process produces errors which vary directly with the interval size differential and amount of variation within the intervals. Comparisons of the limiting

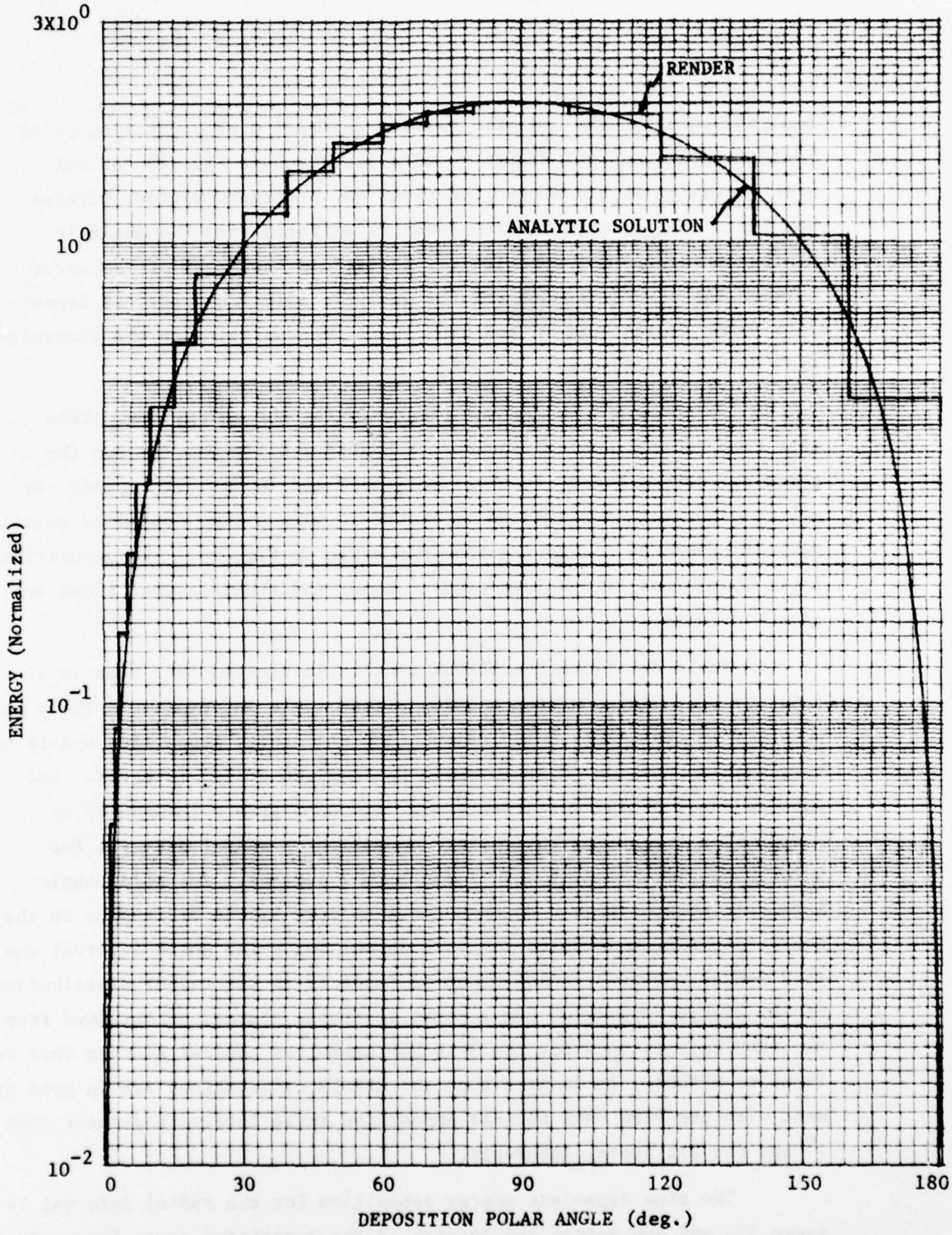

Fig. 12. Comparison of Total Energy Deposition versus Deposition Polar Angle as given by RENDER and Analytic Solution for Sample Problem. Source Emission for Conical Sources between 0° and 90°

analytic results, the analytic results averaged over deposition polar angle interval and the RENDER results are shown in Fig. 13 for the sample problem as the smooth function, the histogram without circles and the histogram with circles (when it differed from the analytic histogram results), respectively. It is seen that most of the error between the RENDER results and the analytic solution occurs at deposition polar angles near 0° and 180° where interpolation on the transmission data was required in RENDER.

To check out the RENDER program using the energy deposition data computed for conical sources, a RENDER problem was run for the gamma ray source energy interval between 9 and 10 MeV. The gamma ray source was taken in RENDER to be isotropic with a time dependent emission rate described by the source function given in Fig. 14. The deposition angle bounds and time values used to print the RENDER calculations are given in Table XIV.

Table XV. lists the RENDER results integrated over time as a function of radial position and deposition angle interval. If there were no error in the RENDER calculation, then the energy deposition should not vary with deposition angle interval for a given radial interval. The data in Table XV indicate that there were some errors introduced by RENDER when evaluating the energy deposition vs radial distance for polar angle intervals of 0 to 1 and 1 to 2 degrees. For polar angle intervals greater than 2 degrees there is very little difference in the energy deposition computed for each deposition polar angle interval and each radial interval. Also shown in Table XV is the radial distribution of the energy deposition for a point isotropic source, as obtained from the DEPO calculations for the 9-10 MeV gamma ray conical sources that were input to RENDER. It is seen that the RENDER calculations are in good agreement with the DEPO data for all deposition angle intervals greater than 2^{o} and for all radial intervals.

The time dependent energy deposition for the radial interval between 350 and 400 meters and in each of the deposition angle intervals is

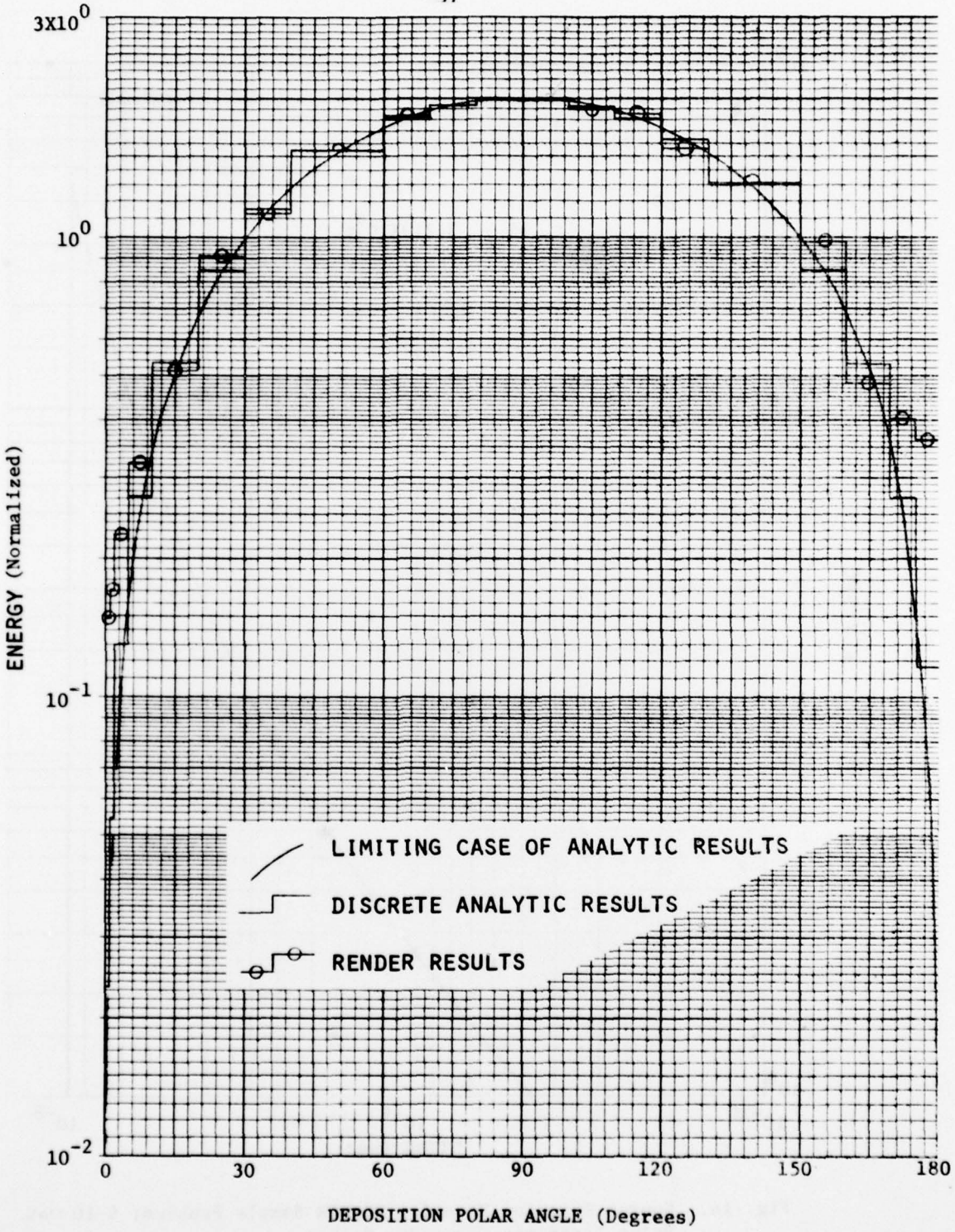

Fig. 13. Comparison of Total Energy Deposition given by RENDER and Analytic Solution for Test Problem: Source Emission for Conical Sources between 0° and 180°

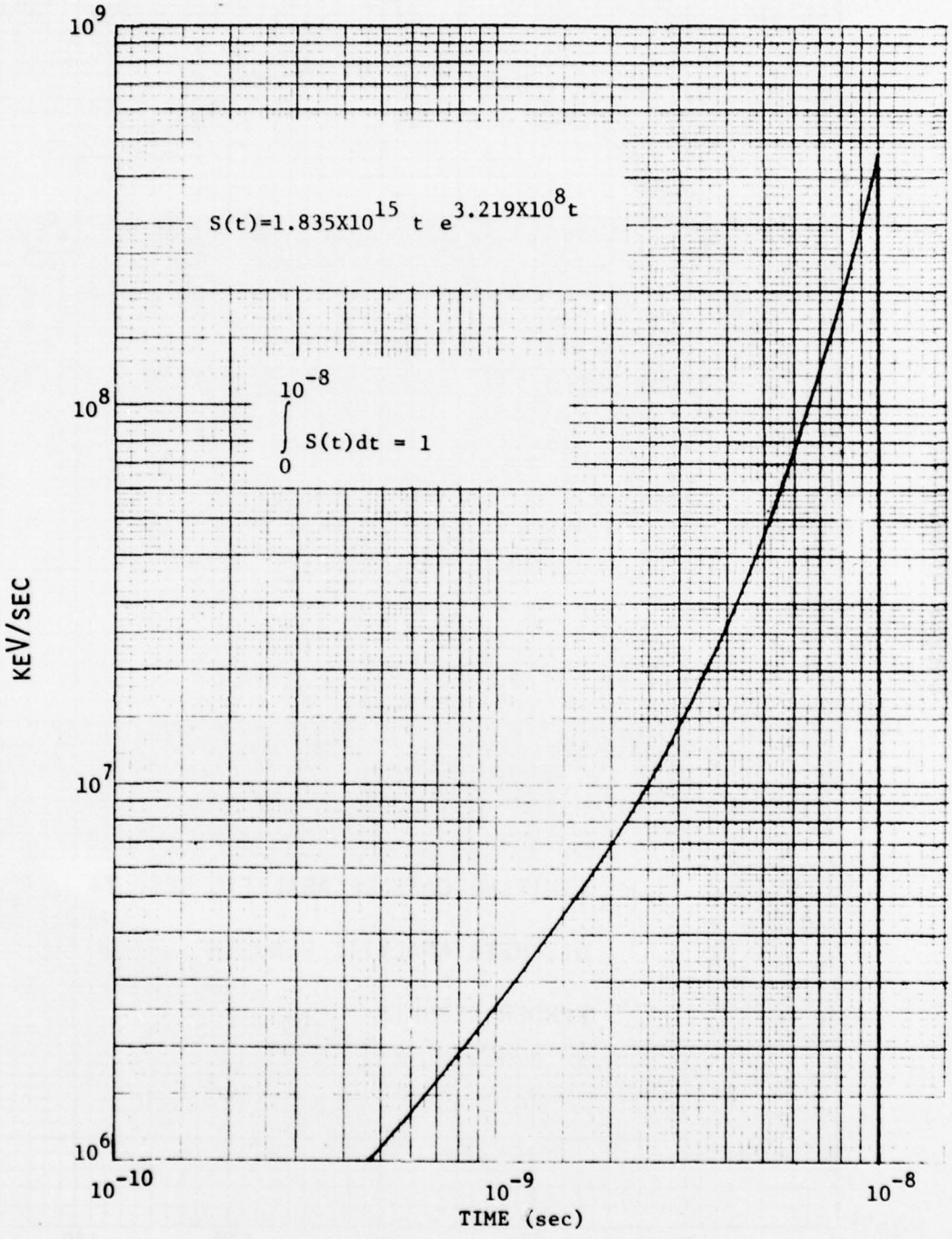

Fig. 14. Source Emission Rate for RENDER Sample Problem: 9-10 MeV Point Isotropic Gamma-Ray Source

TABLE XIV. DEPOSITION TIMES AND POLAR ANGLE BOUNDS USED IN SAMPLE RENDER CALCULATION FOR A POINT ISOTROPIC 9 TO 10 MeV GAMMA-RAY SOURCE

DEPOSITION TIMES (sec)		DEPOSITION POLAR ANGLE BOUNDS (deg)
1.000 - 10	9.900 - 9	0 - 1
5.000 - 10	1.000 - 8	1 - 2
7.000 - 10	1.000 - 8	2 - 50
8.000 - 10	1.758 - 8	50 - 90
9.000 - 10	2.330 - 8	90 - 120
1.000 - 9	3.089 - 8	120 - 150
2.000 - 9	4.095 - 8	150 - 180
3.000 - 9	5.429 - 8	
3.500 - 9	7.197 - 8	
4.000 - 9	9.541 - 8	
4.500 - 9	1.265 - 8	
5.000 - 9	1.677 - 7	
5.500 - 9	2.223 - 7	
6.000 - 9	2.947 - 7	
6.500 - 9	3.907 - 7	
7.000 - 9	5.180 - 7	
7.500 - 9	6.867 - 7	
8.000 - 9	9.102 - 7	
8.300 - 9	1.207 - 6	
8.600 - 9	1.600 - 6	
8.900 - 9	2.121 - 6	
9.100 - 9	2.812 - 6	
9.200 - 9	3.728 - 6	
9.300 - 9	4.942 - 6	
9.400 - 9	6.551 - 6	
9.500 - 9	8.685 - 6	
9.600 - 9	1.151 - 5	
9.700 - 9	1.526 - 5	
9.750 - 9	2.024 - 5	
9.800 - 9	2.683 - 5	
9.850 - 9	3.557 - 5	

TABLE XV. RENDER-CALCULATED TIME-INDEPENDENT ENERGY DEPOSITION DATA FOR A 9 TO 10 MeV POINT ISOTROPIC GAMMA-RAY SOURCE

($keV\ m^{-3}$/keV of source energy)

UPPER RADIAL BOUNDS (METERS)	DEPOSITION POLAR ANGLE INTERVAL UPPER ANGLE BOUNDS (DEGREES)							
	1.00[c]	2.00	50.00	90.00	120.00	150.00	180.00	DEPO
10.0[b]	6.17E-06[a]	5.49E-06	4.69E-06	4.68E-06	4.67E-06	4.70E-06	4.65E-06	4.69E-06
20.0	3.45E-07	7.41E-07	6.46E-07	6.45E-07	6.46E-07	6.46E-07	6.44E-07	6.45E-07
40.0	1.47E-07	1.48E-07	1.53E-07	1.53E-07	1.54E-07	1.53E-07	1.53E-07	1.54E-07
60.0	7.25E-08	6.40E-08	5.53E-08	5.54E-08	5.54E-08	5.54E-08	5.54E-08	5.55E-08
80.0	2.67E-08	2.80E-08	2.87E-08	2.86E-08	2.86E-08	2.86E-08	2.87E-08	2.87E-08
100.0	1.24E-08	1.76E-08	1.54E-08	1.54E-08	1.54E-08	1.54E-08	1.54E-08	1.55E-08
125.0	7.95E-09	1.05E-08	1.00E-08	1.00E-08	1.00E-08	1.01E-08	1.00E-08	1.00E-08
150.0	6.01E-09	6.73E-09	6.15E-09	6.15E-09	6.15E-09	6.16E-09	6.15E-09	6.15E-08
175.0	4.69E-09	4.46E-09	4.43E-09	4.43E-09	4.44E-09	4.42E-09	4.43E-09	4.45E-09
200.0	2.14E-09	2.63E-09	3.13E-09	3.13E-09	3.13E-09	3.13E-09	3.13E-09	3.14E-09
250.0	2.15E-09	2.07E-09	1.95E-09	1.95E-09	1.95E-09	1.95E-09	1.95E-09	1.95E-09
300.0	8.93E-10	1.40E-09	1.28E-09	1.28E-09	1.28E-09	1.28E-09	1.28E-09	1.29E-09
350.0	6.25E-10	8.51E-10	8.14E-10	8.14E-10	8.15E-10	8.13E-10	8.17E-10	8.17E-10
400.0	4.83E-10	6.63E-10	5.58E-10	5.59E-10	5.60E-10	5.57E-10	5.57E-10	5.61E-10
450.0	3.13E-10	4.03E-10	3.77E-10	3.74E-10	3.75E-10	3.75E-10	3.77E-10	3.77E-10
500.0	3.04E-10	2.72E-10	2.93E-10	2.92E-10	2.92E-10	2.93E-10	2.92E-10	2.94E-10
600.0	1.62E-10	1.80E-10	1.84E-10	1.84E-10	1.84E-10	1.83E-10	1.84E-10	1.85E-10
800.0	7.73E-11	8.69E-11	8.30E-11	8.29E-11	8.29E-11	8.28E-11	8.32E-11	8.33E-11
1000.0	3.66E-11	2.68E-11	3.19E-11	3.20E-11	3.20E-11	3.19E-11	3.18E-11	3.21E-11
1200.0	1.80E-11	1.30E-11	1.39E-11	1.39E-11	1.39E-11	1.39E-11	1.39E-11	1.40E-11
1500.0	5.50E-12	4.94E-12	5.33E-12	5.33E-12	5.33E-12	5.34E-12	5.33E-12	5.34E-11

a. Read 6.17E-06 as 6.17×10^{-6}

b. Lower bound of first radial interval = 0 meters

c. Lower bound of first deposition polar angle interval = 0°

given in Table XVI for times less than $5.429X10^{-8}$ seconds. Again it is seen that the energy deposition rate at any given time interval for deposition polar angle intervals less than 2^{o} differs somewhat from the data for deposition polar angle intervals greater than 2^{o}. For deposition polar angles greater than 2^{o} there is very little variation in the energy deposition rate in a given radial interval with deposition polar angle, as expected.

The energy deposited in the atmosphere for print times less than $1X10^{-8}$ seconds as given by the RENDER calculations was found to vary with time in the same manner as does the source function shown in Fig. 14. The RENDER results for times less than 10^{-8} seconds can thus be taken to be made up principally of the energy deposition produced by first order scattering and absorption events. The results of integrating the RENDER data for $150^{o} < \psi \leq 180^{o}$ over time between 0 and 10^{-8} sec are given in Table XVII as a function of the radial interval. Also shown in Table XVII is the energy deposition data for an isotropic source that were obtained from the conical source data that were input to RENDER for 9 to 10 MeV gamma rays in the 0 to 10^{-20} sec retarded time interval. In the conical source data base calculations, the energy deposition occuring in the 0 to 10^{-20} sec retarded time interval came from first order scattering and absorption events. From a comparision of the data in Table XVII, it appears that there is a small contribution by multiple scattering to the RENDER data within the 0 to 10^{-8} sec retarded time interval. This contribution results from the fact that the source in the RENDER calculation emitted radiation over a 10^{-8} sec time interval whereas in the data base calculations the source was assumed to be an instantaneous emitter. The DEPO time dependent energy deposition data input to RENDER indicates that the minimum value of the ratio of the DEPO to RENDER calculations shown in Table XVII should not exceed 0.91. A review of the data in Table XVII reveals that this ratio is always greater than 0.91, as expected.

The time distribution of the energy deposition in the 600 to 800 meter radial interval for times greater than 10^{-8} seconds is shown in Fig. 15. The circled points in Fig. 15 are from the RENDER calculation and the

TABLE XVI. RENDER CALCULATIONS OF THE ENERGY DEPOSITION RATE VS. DEPOSITION POLAR ANGLE INTERVAL FOR A 9 to 10 MeV POINT ISOTROPIC GAMMA-RAY SOURCE IN THE 350 to 400 METER RADIAL INTERVAL

($keV\ m^{-3}\ sec^{-1}$/keV of source energy)

TIME (SEC)	DEPOSITION POLAR ANGLE INTERVAL UPPER POLAR ANGLE BOUNDS (Deg.)						
	1.0	2.0	50.0	90.0	120	150	180
1.000E-10	6.23E-05	9.09E-05	7.21E-05	7.21E-05	7.21E-05	7.21E-05	7.21E-05
5.000E-10	3.56E-04	5.18E-04	4.11E-04	4.11E-04	4.11E-04	4.11E-04	4.11E-04
7.000E-10	5.31E-04	7.75E-04	6.15E-04	6.15E-04	6.15E-04	6.15E-04	6.15E-04
8.000E-10	6.28E-04	9.15E-04	7.26E-04	7.26E-04	7.26E-04	7.26E-04	7.26E-04
9.000E-10	7.30E-04	1.06E-03	8.44E-04	8.44E-04	8.44E-04	8.44E-04	8.44E-04
1.000E-09	8.38E-04	1.22E-03	9.69E-04	9.69E-04	9.69E-04	9.69E-04	9.69E-04
2.000E-09	2.32E-03	3.38E-03	2.69E-03	2.69E-03	2.69E-03	2.69E-03	2.69E-03
3.000E-09	4.83E-03	7.02E-03	5.58E-03	5.58E-03	5.59E-03	5.58E-03	5.58E-03
3.500E-09	6.63E-03	9.64E-03	7.66E-03	7.67E-03	7.67E-03	7.67E-03	7.66E-03
4.000E-09	8.92E-03	1.30E-02	1.03E-02	1.03E-02	1.03E-02	1.03E-02	1.03E-02
4.500E-09	1.18E-02	1.71E-02	1.36E-02	1.36E-02	1.36E-02	1.36E-02	1.36E-02
5.000E-09	1.54E-02	2.24E-02	1.78E-02	1.78E-02	1.78E-02	1.78E-02	1.78E-02
5.500E-09	2.00E-02	2.90E-02	2.31E-02	2.31E-02	2.31E-02	2.31E-02	2.30E-02
6.000E-09	2.56E-02	3.72E-02	2.96E-02	2.96E-02	2.96E-02	2.96E-02	2.96E-02
6.500E-09	3.26E-02	4.73E-02	3.77E-02	3.77E-02	3.77E-02	3.77E-02	3.77E-02
7.000E-09	4.13E-02	5.99E-02	4.77E-02	4.77E-02	4.77E-02	4.77E-02	4.77E-02
7.500E-09	5.20E-02	7.55E-02	6.01E-02	6.01E-02	6.01E-02	6.01E-02	6.01E-02
8.000E-09	6.52E-02	9.46E-02	7.53E-02	7.53E-02	7.53E-02	7.53E-02	7.53E-02
8.300E-09	7.46E-02	1.08E-01	8.61E-02	8.61E-02	8.61E-02	8.61E-02	8.61E-02
8.600E-09	8.51E-02	1.23E-01	9.83E-02	9.83E-02	9.83E-02	9.83E-02	9.83E-02
8.900E-09	9.71E-02	1.41E-01	1.12E-01	1.12E-01	1.12E-01	1.12E-01	1.12E-01
9.100E-09	1.06E-01	1.54E-01	1.22E-01	1.22E-01	1.22E-01	1.22E-01	1.22E-01
9.200E-09	1.11E-01	1.60E-01	1.28E-01	1.28E-01	1.28E-01	1.28E-01	1.28E-01
9.300E-09	1.15E-01	1.67E-01	1.33E-01	1.33E-01	1.33E-01	1.33E-01	1.33E-01
9.400E-09	1.21E-01	1.75E-01	1.39E-01	1.39E-01	1.39E-01	1.39E-01	1.39E-01
9.500E-09	1.26E-01	1.82E-01	1.45E-01	1.45E-01	1.45E-01	1.45E-01	1.45E-01
9.600E-09	1.31E-01	1.90E-01	1.52E-01	1.52E-01	1.52E-01	1.52E-01	1.52E-01
9.700E-09	1.37E-01	1.99E-01	1.58E-01	1.58E-01	1.58E-01	1.58E-01	1.58E-01
9.750E-09	1.40E-01	2.03E-01	1.62E-01	1.62E-01	1.62E-01	1.62E-01	1.62E-01
9.800E-09	1.43E-01	2.07E-01	1.65E-01	1.65E-01	1.65E-01	1.65E-01	1.65E-01
9.850E-09	1.46E-01	2.12E-01	1.69E-01	1.69E-01	1.69E-01	1.69E-01	1.69E-01
9.900E-09	1.49E-01	2.16E-01	1.72E-01	1.72E-01	1.72E-01	1.72E-01	1.72E-01
1.000E-08	1.56E-01	2.26E-01	1.80E-01	1.80E-01	1.80E-01	1.80E-01	1.80E-01
1.000E-08	4.73E-03	5.48E-03	5.32E-03	5.37E-03	5.40E-03	5.30E-03	5.29E-03
1.758E-08	4.73E-03	5.48E-03	5.32E-03	5.37E-03	5.40E-03	5.30E-03	5.29E-03
2.330E-08	4.63E-03	5.39E-03	5.22E-03	5.27E-03	5.30E-03	5.21E-03	5.19E-03
3.089E-08	1.59E-04	9.96E-04	7.18E-04	7.25E-04	7.23E-04	7.20E-04	7.29E-04
4.095E-08	1.59E-04	9.96E-04	7.18E-04	7.25E-04	7.23E-04	7.20E-04	7.29E-04
5.429E-08	1.56E-04	9.58E-04	6.97E-04	7.03E-04	7.01E-04	6.99E-04	7.07E-04

TABLE XVII. COMPARISON OF RENDER AND DEPO DATA FOR ENERGY DEPOSITION RESULTING FROM FIRST ORDER SCATTERING AND ABSORPTION INTERACTIONS

Radial Interval (Meters)	(keV m^{-3}/keV of source energy) RENDER	DEPO
0 - 10	4.25-6*	4.22-6
10 - 20	6.06-7	6.04-7
20 - 40	1.39-7	1.38-7
40 - 60	4.90-8	4.84-8
60 - 80	2.51-8	2.46-8
80 - 100	1.31-8	1.28-8
100 - 125	8.61-9	8.49-9
125 - 150	5.08-9	4.99-9
150 - 175	3.57-9	3.51-9
175 - 200	2.42-9	2.53-9
200 - 250	1.53-9	1.50-9
250 - 300	9.55-10	9.31-10
300 - 350	6.08-10	5.95-10
350 - 400	3.92-10	3.80-10
400 - 450	2.62-10	2.54-10
450 - 500	1.93-10	1.87-10
500 - 800	1.20-10	1.16-10
600 - 800	5.01-11	4.82-11
800 - 1000	1.78-11	1.71-11
1000 - 1200	6.76-12	6.39-12
1200 - 1500	2.33-12	2.18-12

*Read 4.25-6 as 4.25×10^{-6}

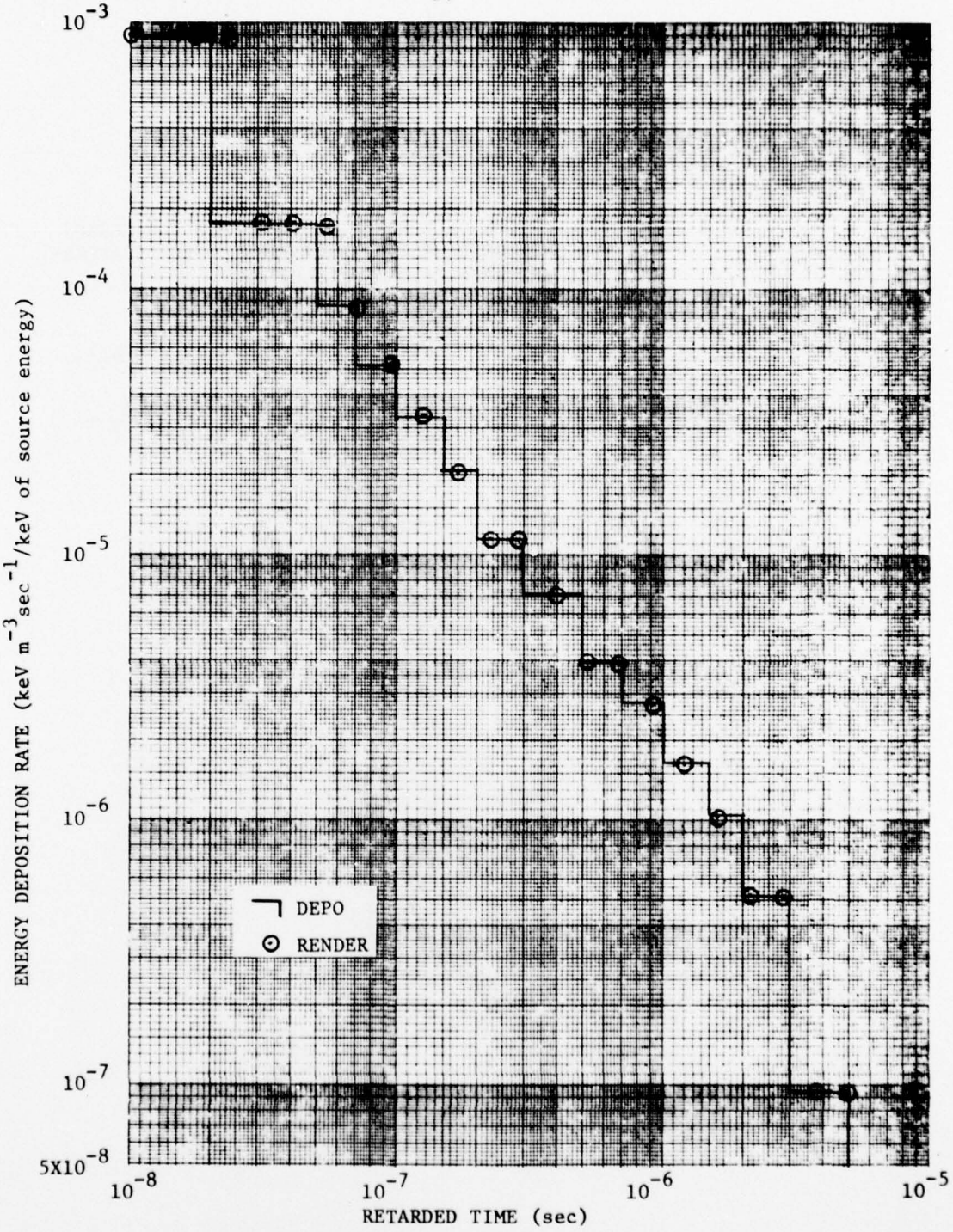

Fig. 15. Comparison between RENDER and DEPO Energy Deposition Rate Calculations for 600 m $<R\leq$ 800 m: Point Isotropic 9-10 MeV Gamma-Ray Source

histogram is from the conical source data input to RENDER. There is good agreement between the two sets of energy deposition data except for times of $2.33X10^{-8}$ sec and $5.42X10^{-8}$ sec. The differences at these times is believed to result from the fact that the energy deposition data input to RENDER was for an instantaneous emitting source and the source used in the RENDER calculation emitted over the time interval between 0 and 10^{-8} sec. Thus the convolution in RENDER of the time dependent source data with the time dependent energy deposition data should result in a slight delay of the energy deposition for times less than 10^{-7} sec.

The good agreement between the RENDER calculations and the conical source data input to RENDER indicates the RENDER procedure is operating correctly. The results of the test problems described above indicate the possible problems that might arise when using RENDER to convolute a time, energy and angle dependent source term with the nuclear energy deposition data base generated for conical sources in this study.

The nuclear energy deposition data base and the RENDER procedure are operational on the CDC-6600 computer at the Los Alamos Scientific Laboratory and on the IBM-360/75 computer at the Air Force Technical Applications Center, Patrick Air Force Base, FL. The RENDER procedure was written in FORTRAN-IV language for each of these computer systems.

REFERENCES

1. J. D. Marshall, M. B. Wells, F. O. Leopard, and K. W. Tompkins, Monte Carlo Procedures for Transport of X-Rays and Fluorescent Light Through a Spherical, Altitude Dependent Atmosphere, Radiation Research Associates, Inc. Technical Report RRA-T94-1 (30 June 1969)

2. J. D. Marshall, Utilization Instructions for ZAPN, A Monte Carlo Neutron Transport Procedure, Radiation Research Associates, Inc. Research Note RRA-N7517 (Sept. 1975)

3. J. D. Marshall, Utilization Instructions for ZAPGAM, A Monte Carlo Secondary Gamma-Ray Transport Procedure, Radiation Research Associates, Inc. Research Note RRA-N7601 (Jan. 1976)

4. D. G. Collins, Utilization Instructions for XORB, A Program to Compute Resonant Absorption and Smog Absorption Cross Sections, Radiation Research Associates, Inc. Research Note RRA-N7501 (February 1975)

5. R. B. Livesay, Photon Cross Sections for 10 ev≤E≤ 100 MeV, Radiation Research Associates, Inc. Technical Report RRA-T7506 June 1975)

6. M. K. Drake (ed.), Data Formats and Procedures for the ENDF Neutron Cross Section Library, Brookhaven National Laboratory, BNL 50274/ENDF102, Vol. I. (Oct. 1970)

7. M. O. Cohen, et al., SAM-CE: A Three-Dimensional Monte Carlo Code for the Solution of the Forward Neutron and Forward and Adjoint Gamma-Ray Transport Equations, Rev. B, Mathematical Applications Group, Inc., Report DNA 2830F-B (August 1973)

8. J. D. Marshall, Utilization Instructions for SGSORC, A Routine for the Generation of Secondary Gamma-Ray Source Parameters, Radiation Research Associates, Inc. Research Note RRA-N7508 (June 1975)

9. M. B. Wells, A Monte Carlo Calculation of Air Scattered Gamma-Ray Dose Rates for Point Monodirectional Sources, Radiation Research Associates, Inc. Technical Report RRA-T7202 (March 1972)

10. R. E. Lynch, J. W. Benoit, W. P. Johnson and C. D. Zerby, A Monte Carlo Calculation of Air-Scattered Gamma Rays, Oak Ridge National Laboratory Technical Report ORNL-2292 (1958)

11. J. H. Price, D. G. Collins and M. B. Wells, Utilization Instructions for SKYSHINE, Radiation Research Associates, Inc. Research Note RRA-N7608 (August 1976)

12. F. H. Clark, "Gamma-Ray Buildup Factors for Sand, Air and Wood (Cellulose)," Nuclear Applications 6:588 (1969)

13. J. H. Hubbell, Photon Cross Sections, Attenuation Coefficients, and Energy Absorption Coefficients from 10 keV to 100 Gev, National Bureau of Standard Report NSRDS-NBS 29 (August 1969)

14. M. B. Wells, Monte Carlo Calculations of Fast Neutron Scattering in Air, General Dynamics Corp., Fort Worth Division, Technical Report NARF-60-8T (FZK-9-147, Vols. I and II); also see M. B. Wells, Gamma Rays from Inelastic Scattering of Neutrons in Air, General Dynamics Corp., Fort Worth Division, Technical Report NARF-60-22T (FZK-9-150) (1960)

15. E. A. Straker, Investigation of the Adequacy of Nitrogen Cross-section Sets: Comparison of Neutron and Secondary Gamma-Ray Transport Calculations with Integral Experiments, Oak Ridge National Laboratory Technical Report ORNL-TM-3768 (Aug. 1972)

16. P. G. Young and D. G. Foster, Jr., An Evaluation of Neutron and Gamma-Ray Production Cross Sections for Nitrogen and A Preliminary Evaluation of the Neutron and Photo-Production Cross Sections of Oxygen, Papers 2 and 3 of a Seminar held Nov. 15-17, 1971, Oak Ridge National Laboratory, Radiation Shield Information Center Report ORNL-RSIC-33 (May 1972)

DISTRIBUTION

No. Copies		No. Copies	
	DOD AGENCIES		DEPARTMENT OF THE NAVY
2	Director Defense Nuclear Agency ATTN: RAAE Technical Library	1	Naval Research Laboratory ATTN: Technical Library
	ENERGY RESEARCH AND DEVELOPMENT ADMINISTRATION		DEPARTMENT OF THE AIR FORCE
3	Los Alamos Scientific Laboratory ATTN: J-10 (Dr. Guy Barasch) TD-3 (Dr. Bob Henson) J-15 (Dr. Gil Davis)	3	AF Geophysical Laboratories ATTN: OPR (H. Gardiner) OPR (Dr. At. T. Stair) OPR (Dr. R. Fenn)
1	Sandia Laboratories ATTN: A. D. Thornbrough	1	AF Institute of Technology ATTN: Library
3	EG&G, Inc. Los Alamos, NM ATTN: D. Wright Dr. K. Mitchell Dr. H. Stewart	3	AF Weapons Laboratory ATTN: Dr. Joe Janni Dr. C. Needham Col. T. W. Ciambrone
1	Lawrence Livermore Laboratory ATTN: Technical Library	2	SAMSO ATTN: SZS (Lt.Col. H. Hayden)
	DEPARTMENT OF THE ARMY	4	AFTAC ATTN: TFR (Capt. Rasmusson)
2	US Army Waterways Experiment Station-Mobility and Environmental System Lab ATTN: Dr. L. E. Link Dr. Warren Grabau		DOD CONTRACTORS
3	US Army Electronics Command Atmospheric Sciences Lab ATTN: Dr. Lewis Duncan Dr. Jerry Lentz Dr. Richard Gomez	5	Radiation Research Associates ATTN: M. B. Wells
		1	Mission Research Corporation ATTN: Technical Library
		1	General Electric Co. - TEMPO ATTN: DNA Information and Analysis Center
		2	Defense Documentation Center ATTN: Document Control